2009

Experimental improvements on a tornado-type wind turbine (TTWT) system

Matt Hawkins
Iowa State University

Experimental improvements on a

tornado-type wind turbine (TTWT) system

by

Matthew Jay Hawkins

A thesis submitted to the graduate faculty

in partial fulfillment of the requirements for the degree of

MASTER OF SCIENCE

Major: Aerospace Engineering

Program of Study Committee:
Fred L. Haan, Jr., Major Professor
Partha P. Sarkar
Tom I-P. Shih

Iowa State University

Ames, Iowa

2009

DEDICATION

This thesis is dedicated to my spouse Amanda, to Peter and Lisa, and to the Aero Boys (and Aero Girl): Ben, Greg, Tom, and Emi. I would like to thank my parents and all of my friends and family for supporting me during my studies and during the writing of this work. Special thanks also go to the British Broadcasting Corporation for outstanding contributions to my non-academic life.

TABLE OF CONTENTS

LIST OF FIGURES

ACKNOWLEDGEMENTS

I would like to take this opportunity to express my thanks to everyone who supported this research and made this thesis possible.

First, Dr. Fred Haan for his guidance and support throughout this research and the writing of this thesis.

I would like to thank Vortex Wind Energy, LLC for sponsoring this research. Special thanks to these members of Vortex Wind Energy, LLC: Steve Dunbar, J. Pierce Scarlett, Bill McClintic, and Jerry Linn.

I would like to give thanks to Dr. Z. J. Wang and his students, Abrar Mohammad and Ying Zhou, for their CFD work with this research.

Finally, I thank Dr. Partha Sarkar, director of ISU's Wind Simulation and Testing (WiST) Laboratory, and Bill Rickard, lab technician for the WiST Lab.

CHAPTER 1. OVERVIEW

Alternative energy sources continue to be of interest to researchers and consumers alike. Wind energy in particular has enjoyed recent growth, albeit mostly on a large scale. The small-scale wind energy design detailed in this paper was first studied in the 1970s, but not enough work has been done to yield a marketable product. Recent advances in wind tunnel instrumentation and computer power enable more sophisticated study of this design. This paper will describe new work on this design, but will start with some background information.

The installation and utilization of wind energy in the United States has exploded in recent years, from a cumulative installed capacity of 2,500 MW at the end of 1999 to a capacity of 16,596 MW by the end of 2007, a growth of 664 percent in eight years. (1) Increased prices for fossil fuels, increased demand for electric power and improved tax credits for renewable energy will fuel continued growth in wind energy. As the technology matures, dropping prices will make wind energy increasingly competitive and further accelerate this growth.

Almost all of the growth in wind energy has come from large-scale commercial wind turbine installations. The size of turbines has also grown significantly. In the early 1980s the largest systems were 50 kW machines with rotor diameters under 20 meters, such as the Kenetech 56 kW 17-meter rotor in Altamont, CA. In March, 2005 a 2.5 MW 93-meter Clipper Windpower turbine was installed in Medicine Bow, WY. (2)

With increased public awareness of wind turbines, home consumers are increasingly interested in installing residential wind energy systems. In 2007, the National Renewable Energy Laboratory, NREL, began a certification for small wind systems. (3) In 2008, The American Wind Energy Association (AWEA) published a residential wind zoning guide for state and local governments. (4) AWEA currently lists over a dozen commercially-proven equipment

providers which together manufacture approximately three dozen small wind systems. (5) All of these systems are essentially smaller-scale versions of the traditional 2- or 3-bladed wind turbine design.

The currently available small wind systems suffer from decreased performance compared to commercially installed systems. This decreased performance is a direct consequence of the theory of wind power extraction, which is also what drives commercial systems to get ever larger and taller. Small wind systems will not enjoy the same increase in popularity and usage if these performance factors are not designed for.

The power available from a wind turbine is governed by the wind energy equation, which says that energy available is proportional to the square of the rotor diameter and the cube of the freestream velocity. The Betz limit says (6) that the efficiency is theortically limited to 59 percent, while mechanical losses often lower the efficiency to around 40 percent.

An atmospheric boundary layer also exists near the earth's surface, caused by the movement of air over the stationary ground. The layer causes a gradient wind profile, with wind velocity quickly increasing with height at lower heights and continuing to slowly increasing to a constant velocity. The velocity does not reach its maximum until a height of well over 1000 feet in urban and suburban areas. This height drops somewhat to no less than 600 feet over open terrain or water.

This combination of factors means that for a traditional wind turbine, power can be increased with larger rotor blades and taller towers. Because residential customers are interested in keeping sizes small, many modifications have been made to the basic design of turbines to increase the effective wind velocity for a given rotor size.

1.1 Previous Work

The Tornado-type wind turbine (TTWT) design was first proposed by Yen (7). The TTWT consists of two parts. The top part is a spiral-shaped chamber, open along the front to allow wind in. The wind that flows into the spiral swirls around and creates a vortex. A vortex creates a low-pressure region at its center. This spiral chamber is mounted on top of a stagnation

chamber which also has an opening allowing wind in through the front. A hole is cut in the interface between the spiral chamber and the stagnation chamber. Figures 1.1 and 1.2 show the basic TTWT configuration. The pressure difference between the low-pressure vortex center and the high-pressure stagnation chamber causes air to flow through the interface and up through the core of the vortex. The continuous inflow of air into the stagnation chamber further drives this process. A fan or other extraction device can be placed in the interface between the chambers to extract power. This configuration allows both pressure energy and kinetic energy to be extracted from wind, while traditional turbines can only extract kinetic energy.

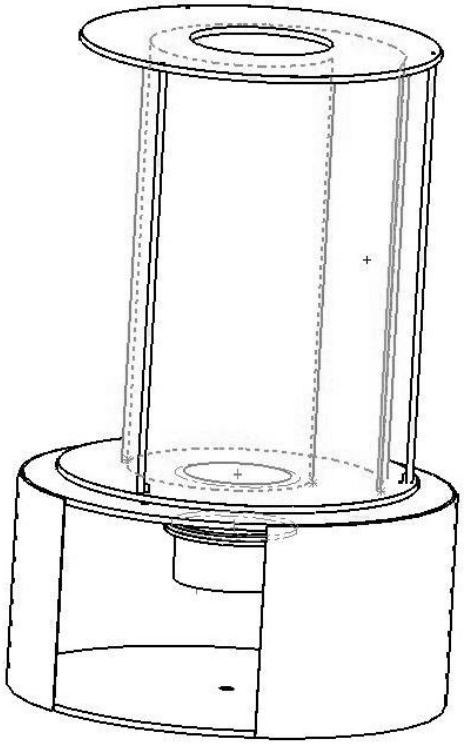

Figure 1.1 Basic TTWT configuration

Yen (8) initially tested only the spiral chamber of the TTWT with a solid flat floor in the chamber. He later tested models with screens in the floor to simulate blockage and momentum loss due to the presence of a turbine, and some models with crude turbines installed in the

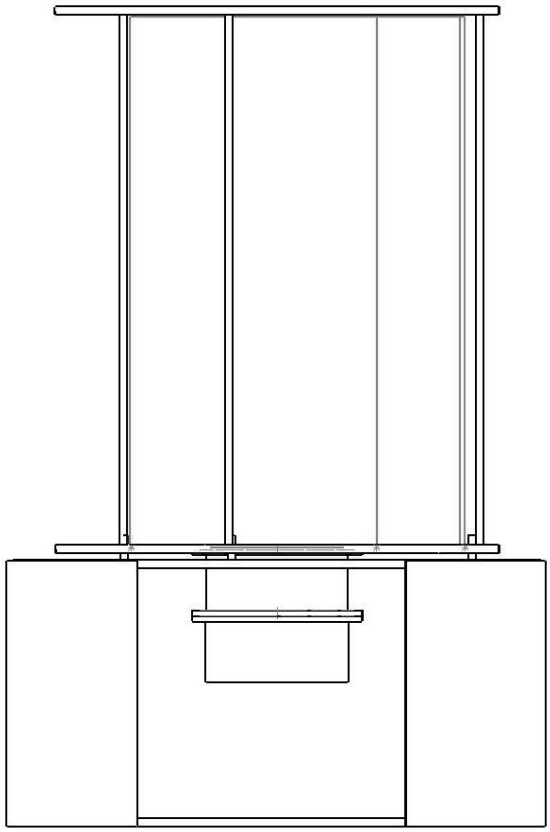

Figure 1.2 Front view of basic TTWT

throat.

Yen also tested omnidirectional models with moveable vanes forming the walls of the vortex chamber. An omnidirectional model is less efficient than a similar-sized fixed spiral facing the wind, however it may be more useful in actual deployment as the chamber does not need to be re-oriented to face the wind.

Rangwalla (9) investigated the theoretical power available, as well as theoretical velocity and pressure distributions, for a one-cell Burgers-type vortex in a spiral chamber. He concluded that radial inflow (air introduced into the walls of the vortex chamber) into the vortex would strengthen the vortex structure.

Tesfamariam (14) studied general vortex flow normal to a solid surface in a cylinder, similar to the TTWT vortex. He found that appropriate amounts of radial inflow can change the

number of vortex cells, and significantly strengthen the updraft velocity within the vortex.

Ide (10) tested the effects of radial inflow on both the basic TTWT spiral shape and a similar model with a circular cross-section. He discovered that radial inflow is more effective on a circular model than on the spiral model, but that the spiral model performs better overall regardless of radial inflow.

Minachi (6) performed a tests of large-scale models of the TTWT in a real environment. He tested both spiral and circular towers both with and without radial inflow. He showed that radial inflow changes the structure of the vortex. Non-uniform inflow can shift where the center of the vortex is. Too much inflow can break up the vortex structure and weaken the core flow.

1.2 Current Study

This study conducted at Iowa State had two main goal areas. First was to reproduce the results from previous work by Yen, Hsu, Minachi, and others. This was done to verify the validity of the TTWT concept and the results that have been obtained so far. The second goal area was to create and test new improvements to the TTWT.

In addition to the experimental work described here, computational fluid dynamics (CFD) simulation has been performed at Iowa State by Dr. Z. J. Wang and his students, Abrar Mohammad (11) and Ying Zhou.

A number of different experimental measurements were made in this study. The pressure coefficient distribution on the spiral chamber floor for the basic spiral models was measured to compare to previous work. Measurements of velocity vectors inside the spiral chamber were made to visualize and characterize the vortex flow structure. Pressure coefficient distributions and velocities through the throat were measured for complete TTWT systems to test how well the complete system works. The power output available from the complete TTWT system was measured, and compared with the power available in the freestream wind.

1.2.1 Reproduction of Previous Work

The first goal area was to verify the results from previous work. In particular, the pressure coefficient distributions on the floor of the spiral chamber were to be measured. Yen (12), Ide (10), and Minachi (6) all measured pressure coefficient distributions on the floor of the spiral chamber, and these measurements were the most practical to repeat. Other measurements from these studies depended sensitively on experiment-specific parameters like the type of screen or exact shape of nozzle and would not give useful comparisons without matching previous experiments exactly. Models of the spiral chamber were constructed and tested in two different wind tunnels. CFD modeling was also performed for different-sized spiral chambers and wind tunnels.

These models tested the effects of varying the overall size of the chamber, the wind tunnel speed, and the wind tunnel blockage caused by the model. Yen (12) ran pressure coefficient tests at a tunnel speed of 5.7 m/s, and Ide (10) ranged from 2.54 m/s to 6.10 m/s. These tests were run at 5.7 m/s to match Yen's work. Additionally, wind speeds of half and double this were used to show whether the pressure coefficients on the chamber floor are independent of wind speed, as expected for pressure coefficients. Both a small and a large model were tested in both a small and a large wind tunnel. The small model blocked about 1% of the large wind tunnel, and 10% of the small wind tunnel. The large model blocked 10% of the large tunnel, and was too large to fit into the small wind tunnel.

The pressure coefficient plots obtained for the various models showed that there was minimal dependence on either wind speed or tunnel blockage. These plots were almost identical to the plots obtained from the CFD analysis.

The pressure coefficient plots obtained did not, however, match those obtained in Yen's (12) (8) work. The performance parameter of most interest, the pressure drop in the center of the vortex, was reported to be much lower in Yen's studies than those found in this paper. It is unclear why this is. It is thought that the static pressure used in previous studies (10) may have been a pressure tap open to the lab and not the static ports of a pitot-static tube, which would change the scale of the pressure coefficient measurements. Although the precise reason

for this discrepancy is not known, the repeatibility of the current measurements with different models, different wind tunnels, different wind speeds, and CFD analysis shows that the pressure coefficient curves measured can be reported with confidence.

1.2.2 New Improvements

The second goal area was to create and test new improvements to the TTWT. Previously, the primary improvement tested was radial inflow. While this is useful for vortex formation, it is also difficult to implement, particularly in a production model that would be left alone outdoors. Most ideas for radial inflow involve mesh screens, which would be less useful when not kept clear and clean.

1.2.2.1 Stagnation Chamber Improvements

A variety of other improvements to the TTWT were tried. Different sizes and configurations for the stagnation chamber were tested. The stagnation chamber in the Yen design is quite large compared to the spiral chamber, so smaller chambers were tried. It is unclear how much the internal design of the stagnation chamber affects the operation of the TTWT. The Yen design does not specify much about the stagnation chamber design, and some changes to the shape of the stagnation chamber produced large performance changes. The inlet orientation is also important. The inlet must be lined up in the direction of the freestream, and small deviations can cause large losses of power.

Placing some devices in the stagnation chamber helps to guide the air flow. Using flow visualization, it was observed that much of the air travels straight through the front inlet and through the throat. The rest hits the back of the stagnation chamber then circulates in the chamber until eventually pulled up with some of the other airflow through the throat. Quarter-pipe sections placed on the floor of the stagnation chamber improved air flow through the throat, as the air circulating in the stagnation chamber had a smoother path to follow before going through the throat. The quarter-pipe sections are described further in Section 2.4.1.

A small fan placed in the throat provided further evidence of the importance of the shape

of the stagnation chamber. The TTWT model was tested in its full configuration with a fan in the throat to determine the cut-in speed for the particular fan used (the speed at which the fan starts to rotate). Then the stagnation chamber was removed and the spiral chamber was elevated on stilts with air flowing underneath where the stagnation chamber had been. The cut-in speed was determined for the fan in this "floating" spiral chamber. Finally the stagnation chamber alone was tested. As expected, the lowest cut-in speed was for the full TTWT configuration. The stagnation chamber alone had a somewhat higher cut-in speed. The "floating" spiral chamber, with air passing both above and below, never caused the fan to rotate for the range of speeds tested. This shows that the air flowing through the stagnation chamber is important in ultimately driving the TTWT, and not just the vortex drawing air in with the low-pressure vortex center.

1.2.2.2 Spiral Chamber Top Improvements

Lids of various sizes were tested. All lids tested covered the spiral chamber with a circle cut out in the middle. The lids showed improvement in increasing the pressure drop in the spiral chamber alone with a flat floor. However, the lids actually decreased the performance of the full TTWT system with the stagnation chamber installed. Flow visualization showed that the air at the top of the spiral chamber inlet went up and exited immediately. The lid is thought to keep some of the rotating air in the spiral chamber longer, thus strengthening the vortex. Flow visualization was impractical with the full TTWT with a lid installed, so it is unknown just what the lid did to the full system.

Based on the flow visualization for the spiral chamber with no lid, another idea was implemented. Rather than constrict the flow out of the top of the device, the top fourth of the spiral chamber inlet was simply blocked. This created a "virtual lid" effect as the air already swirling in the chamber was now diverted to fill in the area behind the blockage. This allowed the air to flow out of the spiral chamber more uniformly, improving the strength of the vortex.

Previous research has mentioned placing something over the TTWT to utilize the Bernoulli effect. The air flowing between the device and the TTWT would accelerate, causing an ad-

ditional suction effect at the top, drawing the air flowing through the core out of the top of the chamber. To test this effect, a raised quarter-pipe section was placed on top of the spiral chamber. The air flowing under this section is accelerated by the Bernoulli effect, causing suction. At the same time, the air going over the top slows down, creating a dead space for air from the spiral chamber to flow into. This quarter-pipe improved the strength of the vortex.

As the quarter-pipe section described above is complicated, the CFD team was not able to replicate it. Instead they simply extended the front half of the spiral chamber up further than the back half. This showed promising results, so it was tested in the wind tunnel. The effect of the extension is similar to the quarter-pipe, as both cause some accelerated airflow and a dead space for air to flow into. Interestingly, the raised quarter-pipe and the extended spiral both caused nearly the same increase in performance. As the extended spiral is easier to build and model, it should be used instead of the extended quarter-pipe.

The lids, inlet top blockage, quarter-pipe ramp, and extended spiral are described further in Section 2.4.2.

1.2.2.3 Vortex Strength Improvements

To encourage stronger upflow in the bottom of the spiral chamber, a small quarter-pipe ramp was placed at the spiral chamber inlet floor. The ramp was placed in front of the chamber, with the top of the section meeting the plane of the chamber inlet. The ramp was made of a thin material, which allowed for some inflow at the floor. This ramp did not improve the overall average performance, however it improved the structure of the vortex and vortex core. Without the ramp, the updraft velocity of the vortex core varied from low to high in both the cross-stream and downstream directions. With the ramp installed, the velocity distribution was much closer to circularly symmetric. This is much better for fans or other extraction devices, as the forces on the blades will not vary with angular position of the blades.

Different attempts were made to divert more air into the spiral chamber. An airfoil section was placed in front of the spiral chamber inlet, outside the projected area of the spiral chamber. It is thought that diverting more air into the spiral chamber can increase the vortex strength.

However, simply forcing more air into the inlet, for example by diverting with panels, will not necessarily improve performance. As with traditional wind turbines, a "pressure bubble" can form which the freestream air will simply go around. A correctly placed airfoil section showed some modest improvements, but not enough to continue focusing on in the present study.

A small amount of radial inflow was tested. Rather than employ the extensive system of screens and double-layered walls from previous work, these tests simply employed small holes cut out of the spiral chamber wall. These were threaded with tubes to ensure air flowed through the holes. Some placements of radial inflow plugs caused modest improvement, while others showed no change in performance.

The radial inflow tubes and entry scoop are described further in Section 2.4.3.

1.2.2.4 Best Combination of Improvements

Ultimately, a combination of improvements was found representing the best performance observed. This set includes a ramp at the floor of the spiral chamber inlet, blocking the top sixth of the spiral chamber inlet, and extending the upstream part of the spiral chamber. A smaller stagnation chamber with quarter-pipe inserts is used.

CHAPTER 2. TORNADO TYPE WIND TURBINE MODELS: EXPERIMENTAL SETUP AND TESTING SUMMARY

2.1 Introduction

To study the performance of the general tornado-type wind turbine (TTWT) system, two models were constructed and tested separately. The first model included only the spiral tower, while the second model included the spiral tower section, to which a stagnation chamber was later added. This chapter provides details of the construction of these models, as well as descriptions of experimental setups. Various new improvements to the TTWT design are also described.

2.2 14-Inch Spiral Model

The basis of the tornado-type wind turbine design is the low-pressure spiral chamber. This is the part of the machine that creates a contained vortex. The first spiral model (the 14-in.) was constructed of plywood braces with an inside shape defined by $r = r_0 e^{\alpha}$. The braces were held together with three vertical rods for stiffness. A thin stiff wall made of Formica sheeting was installed in the spiral braces to form the spiral chamber wall. A 3D rendering of the spiral chamber can be seen in Figure 2.1. Because the formica sidewall tends to bow out when curled into a spiral, vertical stabilizers were attached to the leading and trailing edges of the wall to keep the wall vertical. In order to allow clean airflow into the chamber, the inner stabilizer was covered with a second layer of material that wraps around the front of the chamber. The vertical stabilizers can be seen in Figure 2.2. It was discovered during testing that these stabilizers interfere with the airflow into the chamber, so they were later replaced

with horizontal rods. Horizontal rods were used for all subsequent models. The horizontal rods can be seen in Figure 2.3.

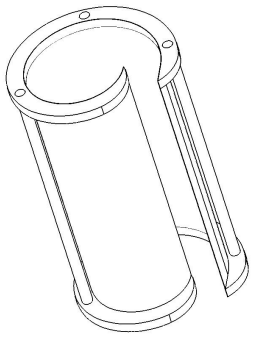

Figure 2.1 14-in. spiral chamber model

In order to measure the pressure drop caused by the vortex, the 14-in. model was tested in the AABL Wind and Gust Tunnel at the ISU Wind Simulation and Testing (WiST) Lab at Iowa State University. This is a closed-circuit tunnel with an 8 foot wide by 6 foot tall aerodynamic test section. The 14-in. model was mounted to a test platform with a sharp leading edge. The model was centered on the platform and located several body lengths back. Figure 2.4 shows the 14-in. spiral model in the wind tunnel, mounted on the test platform. An array of pressure taps were placed in the floor inside the model's footprint. Figure 2.5 shows the installed arrangement of these pressure taps. The floor pressure taps were connected to two Scanivalve 16-channel Digital Sensor Array (DSA) digital pressure scanners. A pitot-static tube upstream of the platform was also connected to the DSA to measure freestream dynamic pressure. The freestream static pressure from the pitot-static tube was used as the reference static pressure on the DSA. Floor pressures were measured at three different wind speeds for both types of stabilizers.

The pressure coefficient used in this paper is defined as:

$$\frac{p - p_\infty}{q_\infty}$$

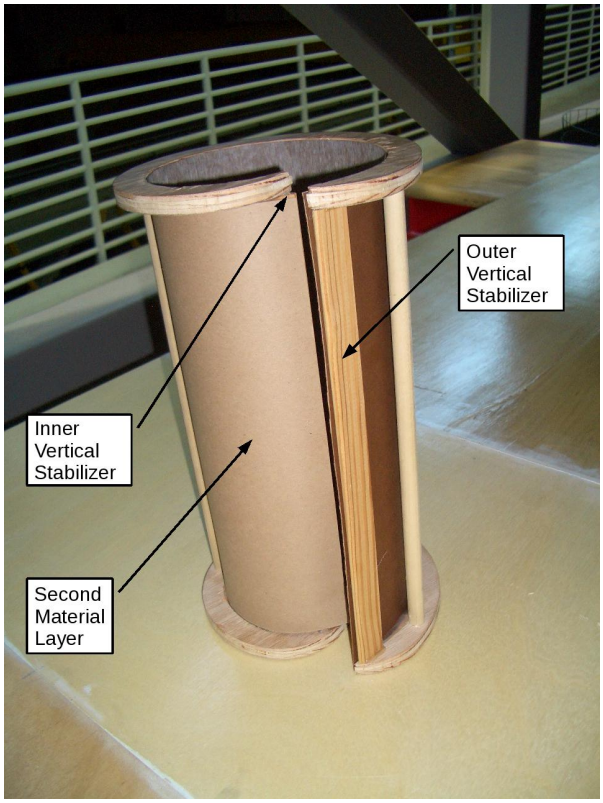

Figure 2.2 Vertical stabilizers shown on 14-in. spiral model

where:

p = the pressure measured at the location of interest, usually the floor pressure tap

p_∞ = the static pressure measured on the upstream pitot-static tube

$q_\infty = p_{total} - p_\infty$

p_{total} = the total pressure measured on the upstream pitot-static tube.

It was thought that wind tunnel blockage effects may have been affecting the results of the floor pressure coefficient measurements. The spiral chamber is clearly not an aerodynamically streamlined body, as it is approximately cylindrical and the capture area is small compared to the projected area. However, because the top of the model is open and all of the captured air exits out of the top, it also behaves quite differently than a bluff body. To measure the effects of wind tunnel blockage, the 14-in. model was also tested in the Bill James wind tunnel in the ISU WiST Lab at Iowa State University. The Bill James wind tunnel is an open-circuit wind tunnel with a 4 foot wide by 3.5 foot tall test section.

Figure 2.3 Horizontal stabilizer rods shown on 14-in. spiral model

2.3 36-Inch Spiral Model

A larger model was constructed to test the effects of scaling the spiral chamber. This model was sized for approximately a 10% blockage of the test cross-section of the Aerodynamic and Atmospheric Boundary Layer (AABL) Wind and Gust Tunnel in the Wind Simulation and Testing (WiST) Laboratory at Iowa State University. The AABL Wind and Gust Tunnel (hereafter also referred to as the AABL tunnel) is a closed-circuit wind tunnel with an 8 foot wide by 6 foot tall aerodynamic test section. The 10% blockage figure was chosen as it is a rough rule of thumb value for maximum cross-sectional blockage to avoid interference effects due to blockage. This is also roughly the blockage caused by the 14-in. model in the Bill James Wind Tunnel.

This larger model was approximately 36 inches tall and constructed of a base and brace made of medium-density fiberboard (MDF) with paperboard walls and steel threaded rod

Figure 2.4 14-in. model in wind tunnel, mounted on test platform, showing pitot-static tube in front

vertical braces. The MDF base and brace were milled by a computer numerical controlled (CNC) router, allowing precise use of the logarithmic spiral shape. Paperboard was chosen for the walls because it afforded sufficient stiffness to maintain the shape of the wall without being too stiff to curl into the spiral shape. Horizontal braces were again used to prevent the inside edge of the wall from bowing out. The 10 percent model can be seen in Figure 2.6. In later tests the paperboard wall was replaced with clear Lexan plastic.

To test the effect of flow through the entire TTWT device, a stagnation chamber was built for the 36-in. model. The top and bottom of the chamber were built out of machined MDF, and the walls were made of paperboard, similar to the 10 percent model. Figure 2.7 shows the stagnation chamber from the back. Figure 2.8 shows the 36-in. model mounted on top of this stagnation chamber. For some tests, described in 3.2.4, the front of the spiral section was blocked off. Figure 2.9 shows the TTWT with stagnation chamber and blocked spiral chamber.

2.4 Improvements to Tornado-Type Wind Turbine Design

2.4.1 Stagnation Chamber Improvements

The baseline model (Yen's design) has a rather large stagnation chamber, with a volume similar to the volume of the spiral chamber. It is not clear that this large of a chamber

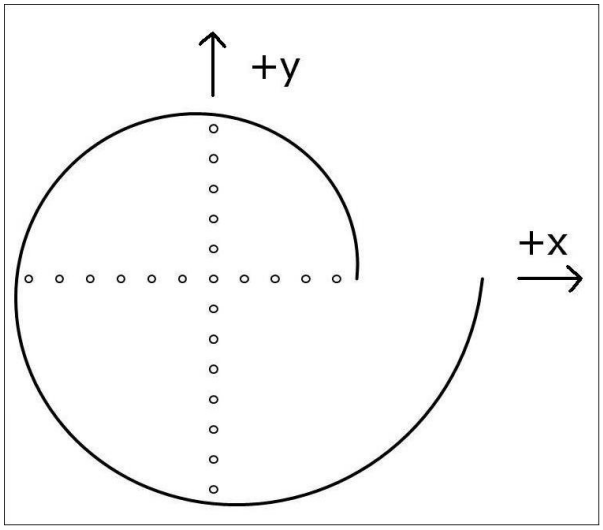

Figure 2.5 Schematic showing pressure tap locations for both 14-in. (r_0 = 5.36 cm) and 36-in. (r_0 = 14.0 cm) models, and coordinate directions

is needed, and thus a smaller stagnation chamber was built. Yen's stagnation chamber was approximately half the height of his spiral chamber and three times the volume. To test the effects of stagnation chamber size, much smaller stagnation chambers were used. The basic new stagnation chamber was simply a smaller cylinder with a rectangular inlet in front. This chamber is shown in Figure 2.10. The performance of this stagnation chamber improved with quarter-pipe sections placed inside to direct airflow upward. The inlet front inlet required extra blockage in front of the front quarter-pipe section to ensure smooth airflow. Figure 2.11 shows the placement of these quarter-pipe sections.

2.4.2 Spiral Chamber Top Improvements

Ide (10) tested lids with different sizes of openings. Similar lids were tested on the 36-in. spiral. Several different hole sizes were tried. Figure 2.12 shows a schematic of some of the different possible hole sizes for the lid. The hole in the lid was always centered on the center of the spiral geometry. This type of lid showed improvements for the pressure drop of the spiral chamber by itself, but did not show improvements when applied to the complete TTWT design.

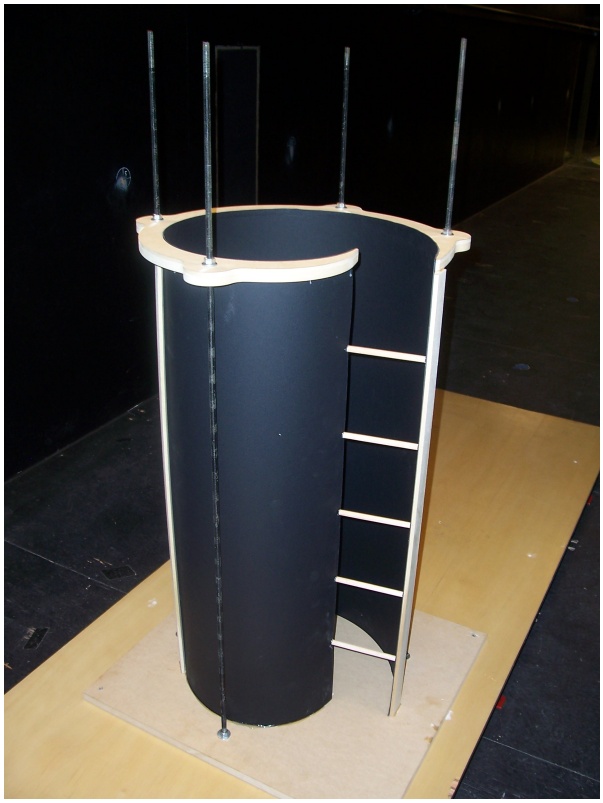

Figure 2.6 36-in. model

A ramp device was placed on top of the spiral chamber to take advantage of the Bernoulli effect. This ramp was designed to create suction by accelerating air flow over the top of the spiral chamber. CFD simulation showed that a similar effect could be achieved by merely extending the front of the spiral chamber higher instead of using a ramp. This is much easier to construct and modify and should be utilized in future work. A small blockage of the top of the spiral chamber inlet also increased TTWT performance. Figure 2.13 shows both top devices as well as the front inlet blockage.

2.4.3 Vortex Strength Improvements

Instead of an extensive side screen system, radial inflow was provided by simple tubes installed in the spiral chamber wall. These tubes must be aligned in the direction of the freestream to provide additional air into the spiral chamber. A small ramp on the floor of the inlet also allows modified airflow into the chamber near the interface between the spiral and

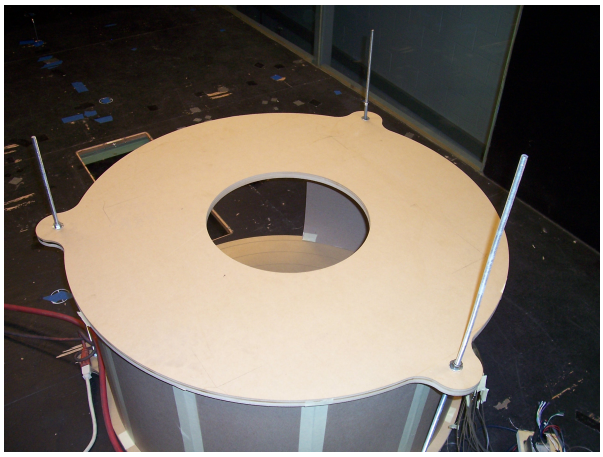

Figure 2.7 Close-up of top of stagnation chamber

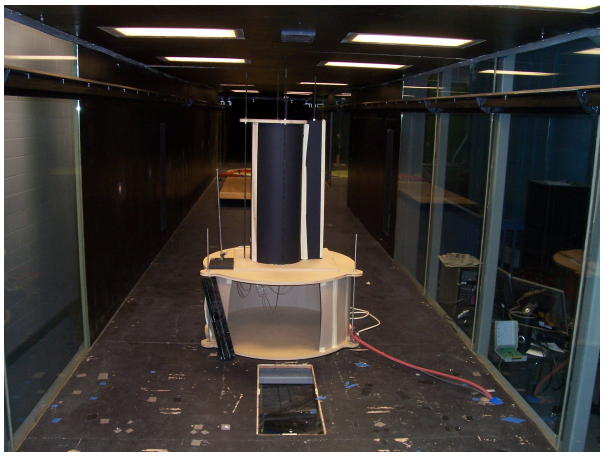

Figure 2.8 36-in. model on top of stagnation chamber

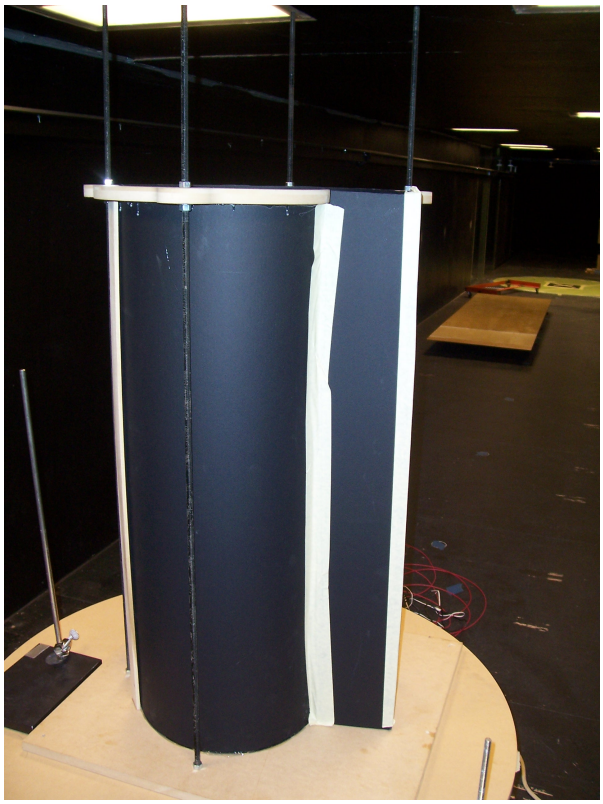

Figure 2.9 Spiral chamber inlet blockage to measure “chimney effect”

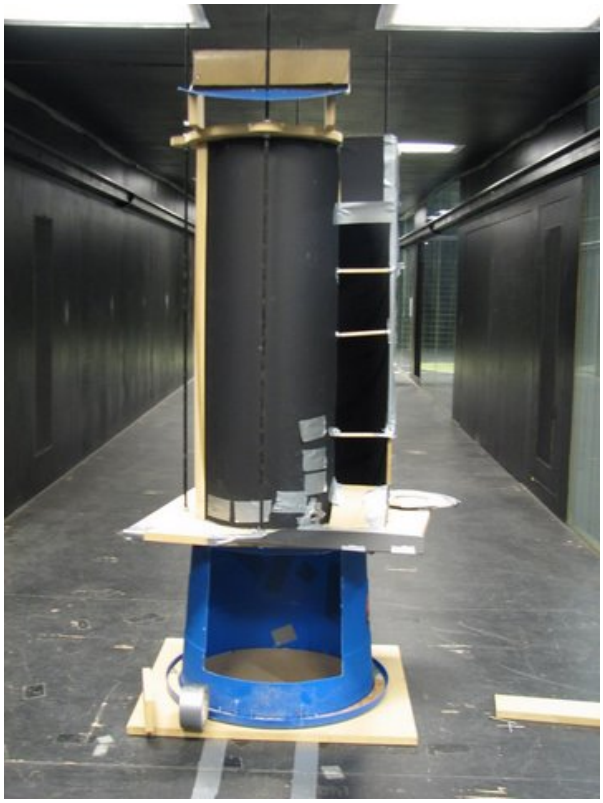

Figure 2.10 Basic smaller stagnation chamber design shown under modified spiral chamber
Design modification and fabrication by J. Pierce Scarlett, photo courtesy J. Pierce Scarlett

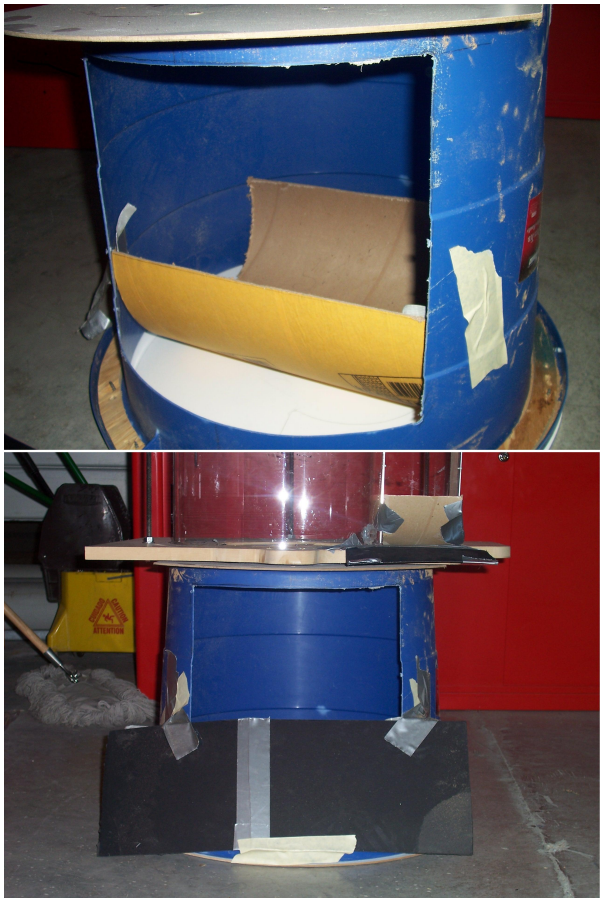

Figure 2.11 Top: Quarter-pipe sections in the small stagnation chamber Bottom: Extra blockage in front of quarter-pipe sections Design modification and fabrication by J. Pierce Scarlett, photos courtesy J. Pierce Scarlett

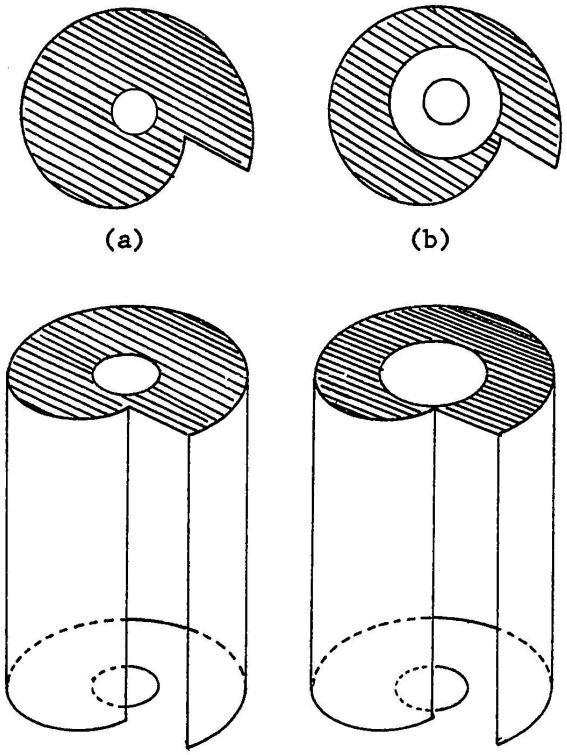

Figure 2.12 Schematic of spiral chamber lid geometry (adapted from Ide (10))

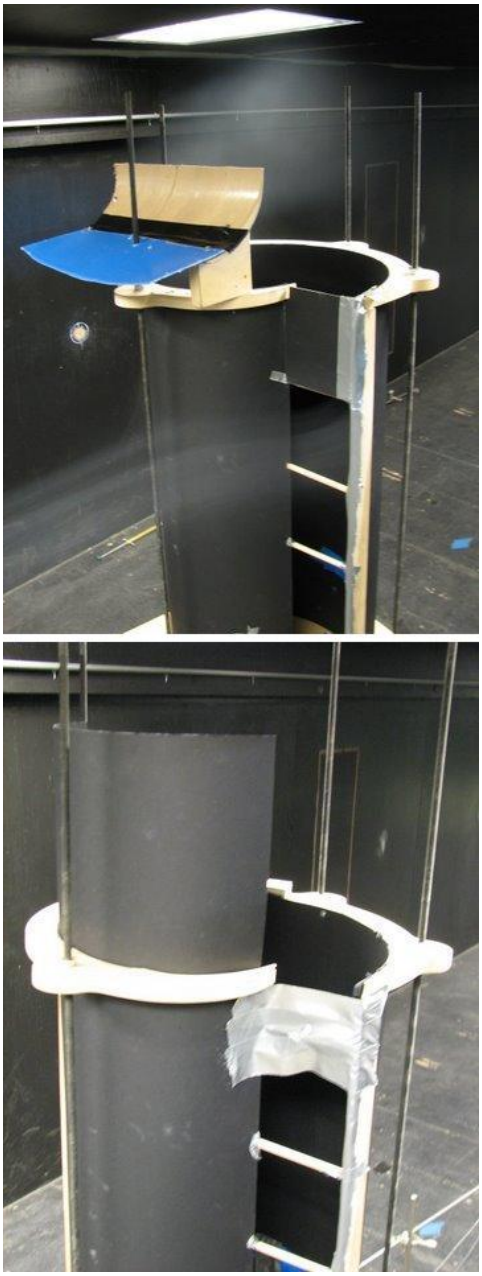

Figure 2.13 Top: Extended ramp on top of spiral with top inlet blockage shown
Bottom: Extended spiral chamber wall with top inlet blockage shown
Design modification and fabrication by J. Pierce Scarlett, photos courtesy J. Pierce Scarlett

stagnation chambers. Figure 2.14 shows different configurations for the radial inflow tubes as well as the front entry ramp.

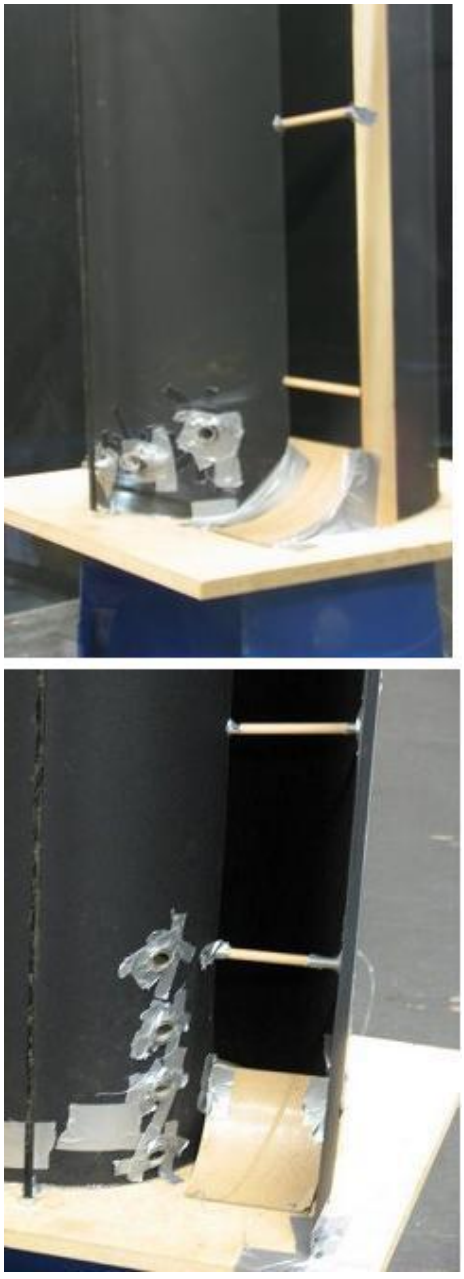

Figure 2.14 Top: Horizontal radial inflow tubes shown with front entry ramp
Bottom: Vertical radial inflow tubes shown with front entry scoop
Design modification and fabrication by J. Pierce Scarlett, photos courtesy J. Pierce Scarlett

CHAPTER 3. RESULTS

Results of wind tunnel measurements are given in this chapter. Measurements of the pressure coefficients in the various models are given, as well as measurements of velocities inside the spiral chamber. Pressure coefficients and velocities are given for a complete TTWT system (stagnation chamber and spiral chamber). Finally, measurements of the power output from the best combination of model parameters are compared with the power available in the freestream wind.

3.1 14-Inch Model

The 14-in. model was tested in the AABL Wind and Gust Tunnel in the WiST Lab. The pressure coefficients measured on the floor of the model with vertical stabilizers are shown in Figures 3.1 and 3.2. These figures show a moderate drop in pressure coefficient, down to as low as -1.5 in the center of the vortex. The figures clearly show a vortex structure, with pressure drop peaking in the center and decreasing out to the walls. The figures also demonstrate minimal dependence on velocity over a range of velocities.

It was thought that the vertical stabilizers interfered with clean capture of air in the front of the spiral. The vertical stabilizers were replaced with horizontal stabilizers as described in Section 2.2. The pressure coefficients measured with horizontal stabilizers installed are shown in Figures 3.3 and 3.4. These figures show that the pressure drop in the center is bigger than before, and is still independent of velocity.

The 14-in. model was also tested in the smaller Bill James Wind Tunnel in the WiST Lab. Pressure coefficients measured in these tests are shown in Figures 3.5 and 3.6. These figures look similar to the previous pressure coefficient plots (Figures 3.1 through 3.4). The pressure

drop in the center is approximately 25% greater than the previous drop. This may be due to wind tunnel blockage effects. The model blocks approximately 10% of the cross-section of the Bill James tunnel, compared to blocking approximately 1% of the AABL cross-section.

The Reynolds number (based on r_0) for 14-in. model tests ranged from approximately 9200 for the smallest velocity to 42,000 for the highest velocity. The Reynolds number for flow at 5.7 m/s is approximately 20,000.

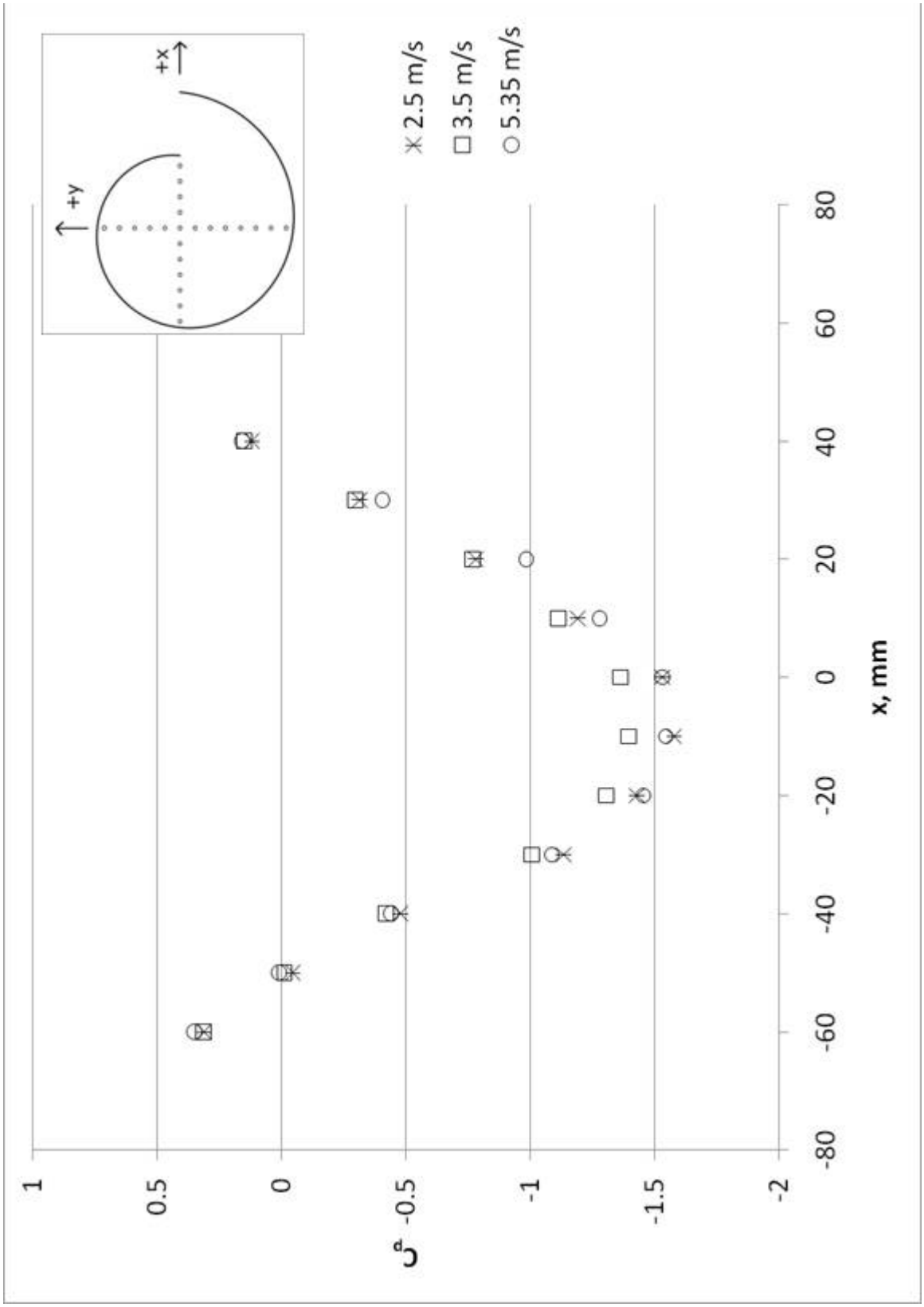

Figure 3.1 Y-axis pressure coefficients, 14-in. model with vertical stabilizers, AABL wind tunnel, three wind speeds

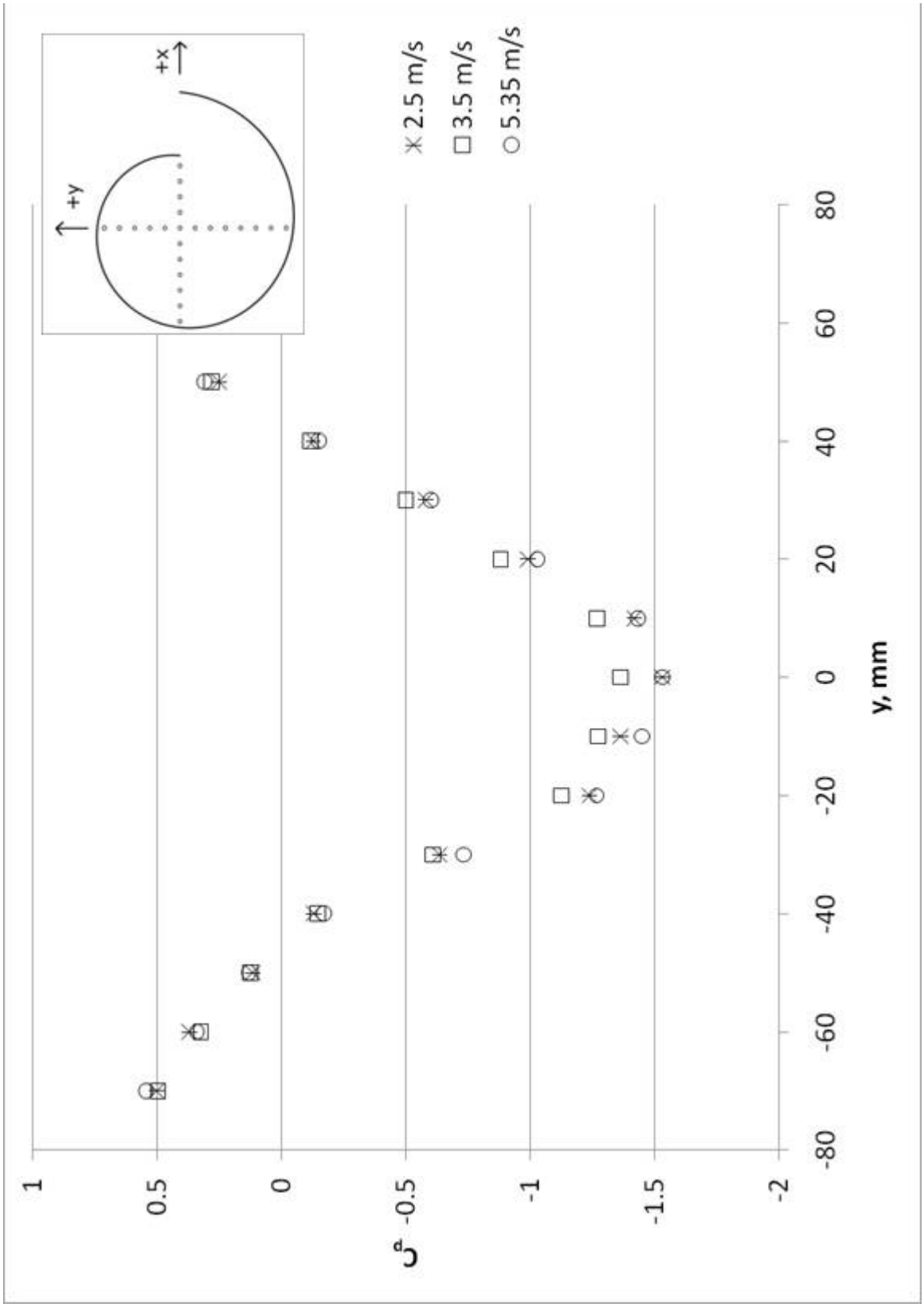

Figure 3.2 X-axis pressure coefficients, 14-in. model with vertical stabilizers, AABL wind tunnel, three wind speeds

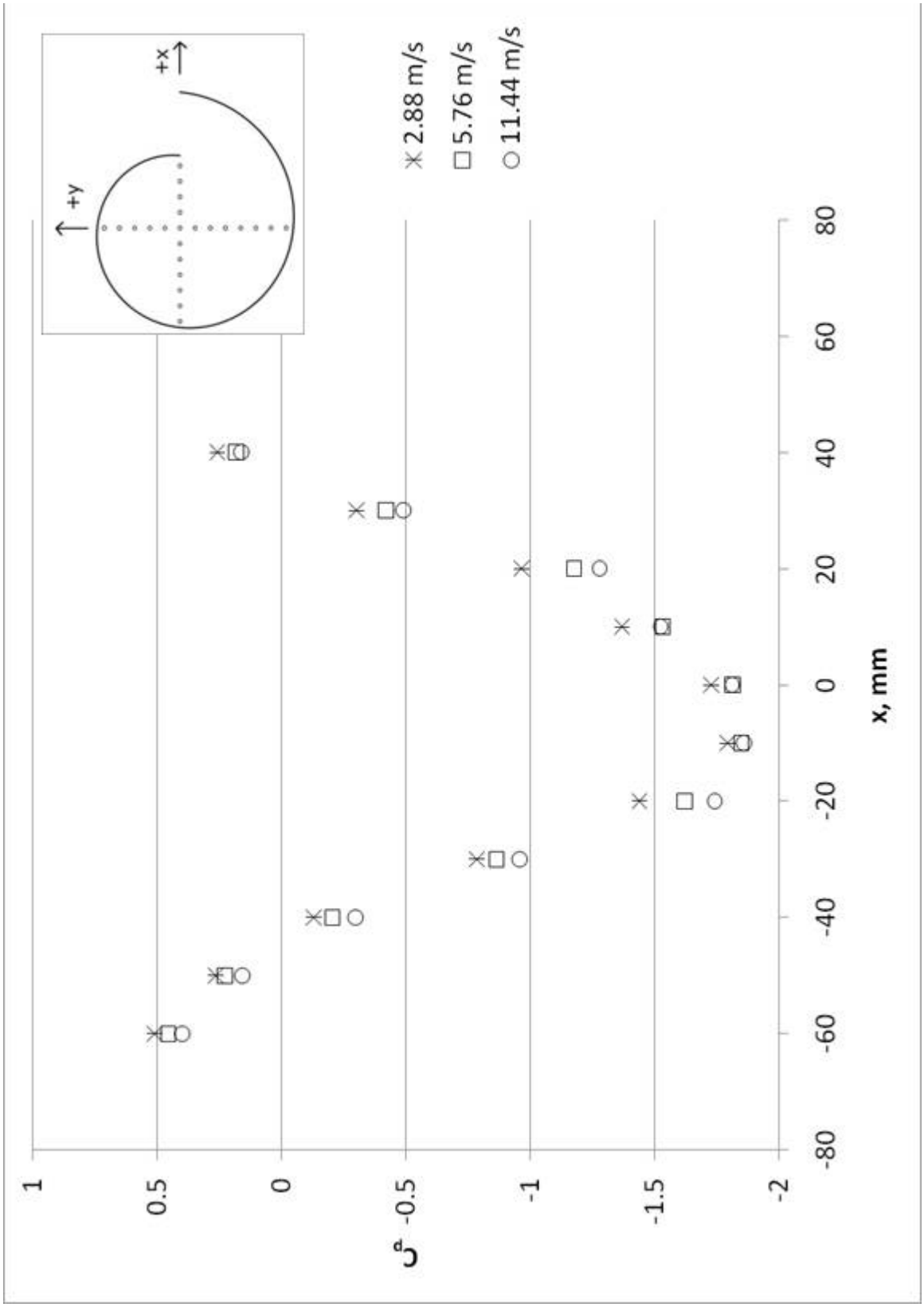

Figure 3.3 Y-axis pressure coefficients, 14-in. model with horizontal stabilizers, AABL wind tunnel, three wind speeds

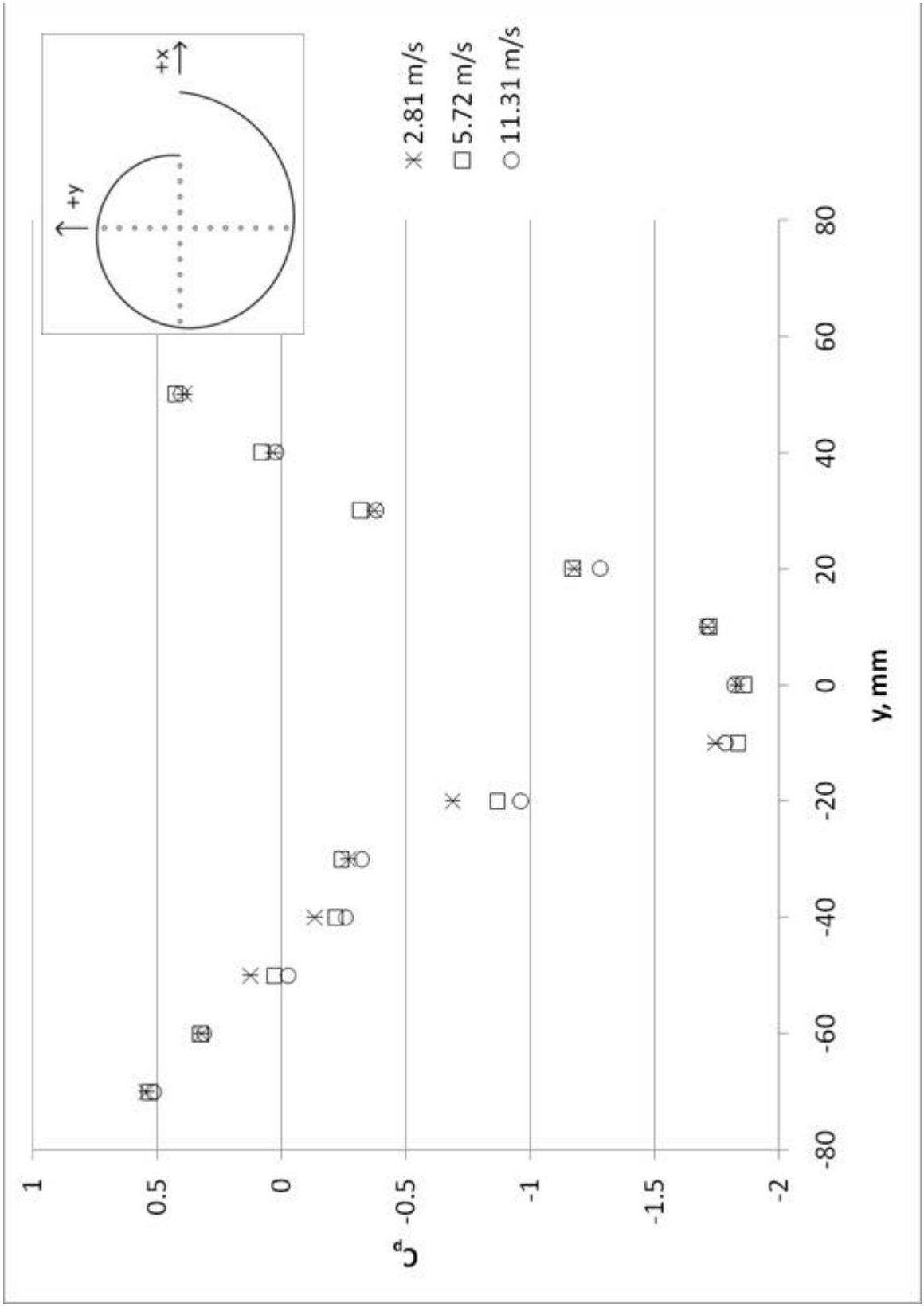

Figure 3.4 X-axis pressure coefficients, 14-in. model with horizontal stabilizers, AABL wind tunnel, three wind speeds

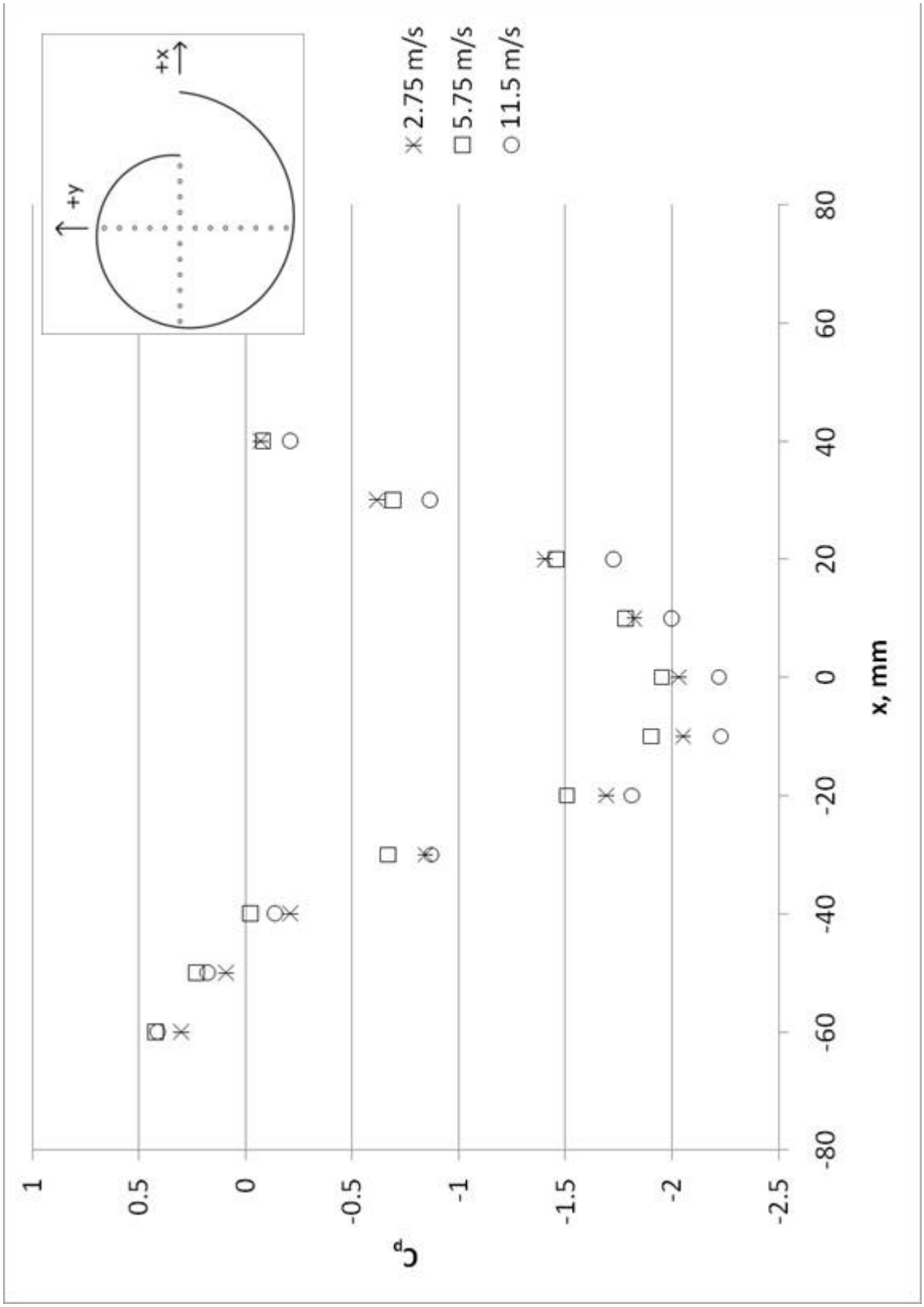

Figure 3.5 Y-axis pressure coefficients, 14-in. model with horizontal stabilizers, Bill James wind tunnel, three wind speeds

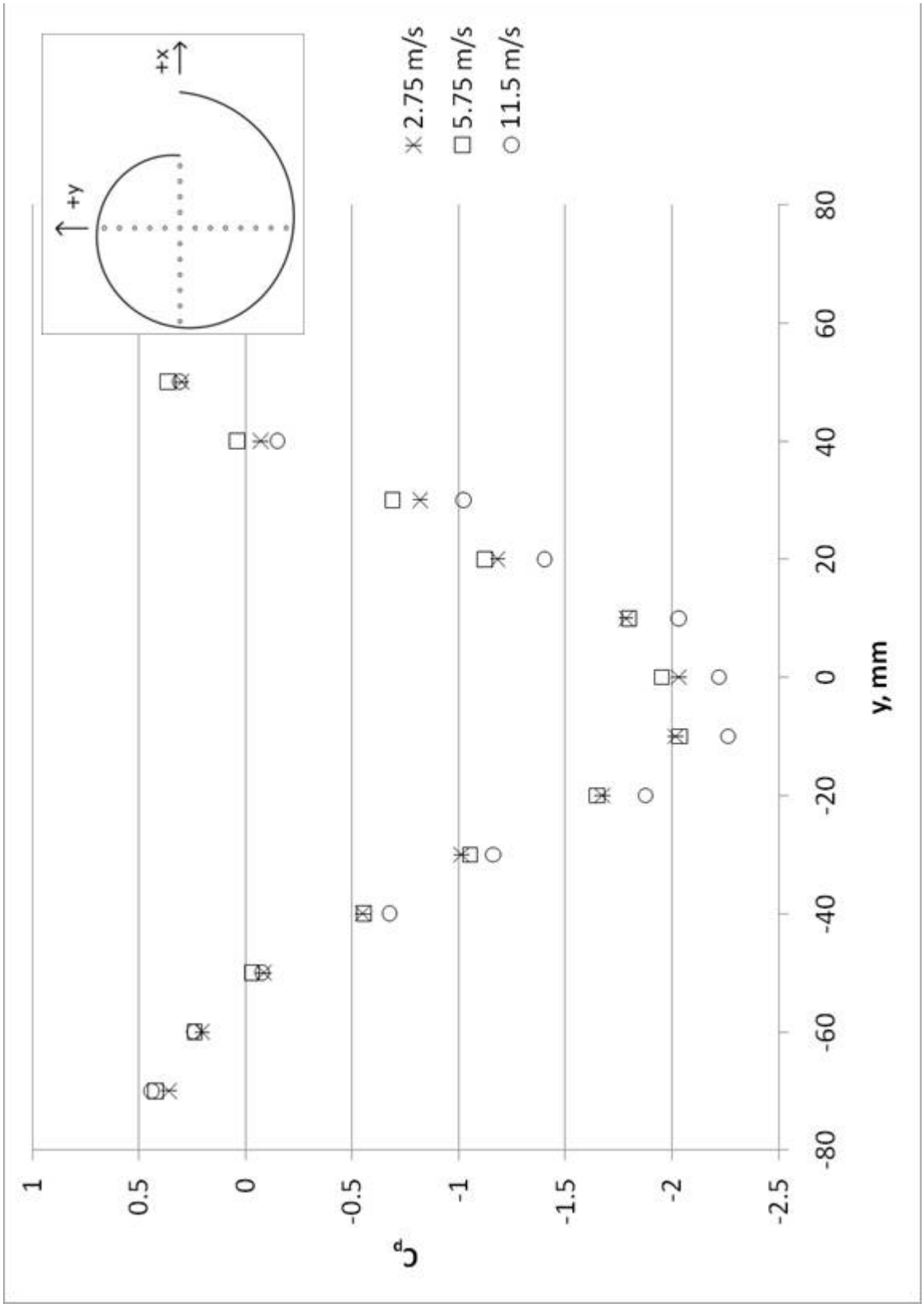

Figure 3.6 X-axis pressure coefficients, 14-in. model with horizontal stabilizers, Bill James wind tunnel, three wind speeds

3.2 36-Inch Model

The spiral section of the 36-in. model was tested in the AABL Wind and Gust Tunnel. Meausured floor pressure coefficients are shown in Figures 3.7 and 3.8. The pressure drop for this model is again low in the middle, suggesting stronger vortex formation.

The averaged pressure coefficients for the 10 percent model, the 14" model with horizontal stabilizers, and computational fluid dynamics (CFD) simulations are shown in Figures 3.9 and 3.10. These figures show agreement within at most 30% in the basic shape of the pressure coefficient curve across a variety of model sizes, wind tunnel sizes, and CFD simulations. The pressure coefficient curves agree within 25% for the 14-in. model. These figures demonstrate that the vortices formed are relatively independent of model size and wind speed.

The Reynolds number (based on r_0) for the 36-in. model is approximately 55,000.

3.2.1 Flow Inside the Spiral Chamber

In order to characterize the flow inside the spiral chamber, three-dimensional velocity vectors were measured inside the spiral chamber with an Omniprobe multi-hole pitot-static probe. The omniprobe is a small brass sphere with eighteen pressure taps machined into the sphere forming a network of six interconnected five-hole pitot static probe arrays. The Omniprobe tip can be seen in Figure 3.11. A proprietary curve-fitting software program converts the pressure measurements to a three-dimensional flow vector.

Velocity vectors in the spiral chamber were measured with the Omniprobe. One-minute average velocity measurements were made at nine cross-stream points and eleven downstream points at heights of z/L=.222, .444, and .667. Figure 3.12 shows the horizontal plane velocity vectors at three different heights. The origin point was measured on both the across-stream and downstream measurement passes. Due to minor interference effects from the presence of the omniprobe, there are two slightly different velocity vectors at the origin.

The horizontal in-plane velocities show circular rotation as expected. The center of rotation is close to the center of the coordinate system, as the velocity vectors all rotate about that point. The small velocity vectors at the origin show that the rotation velocity at the origin

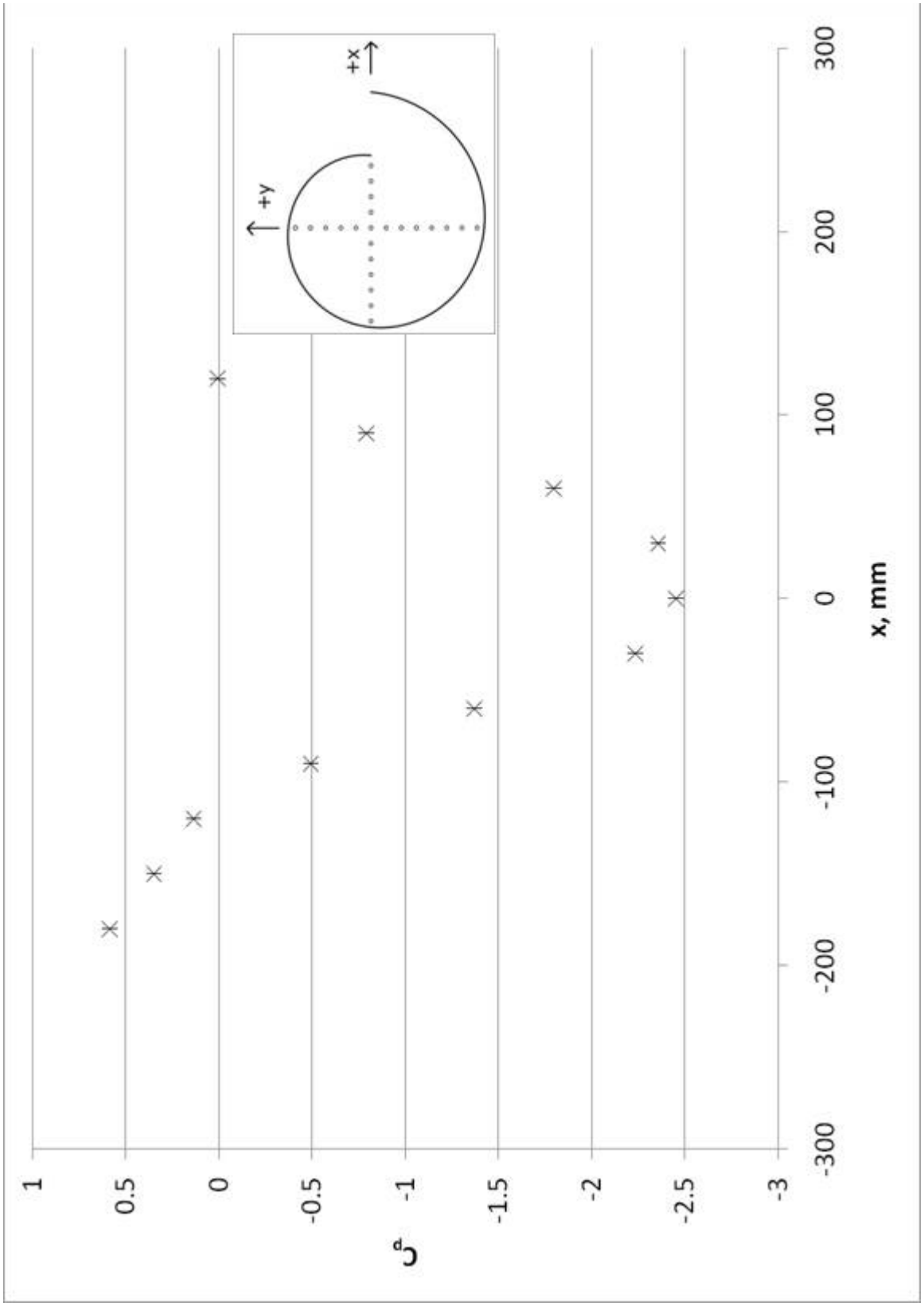

Figure 3.7 Y-axis pressure coefficients, 36-in. model spiral chamber with flat floor, AABL wind tunnel, 5.7 m/s

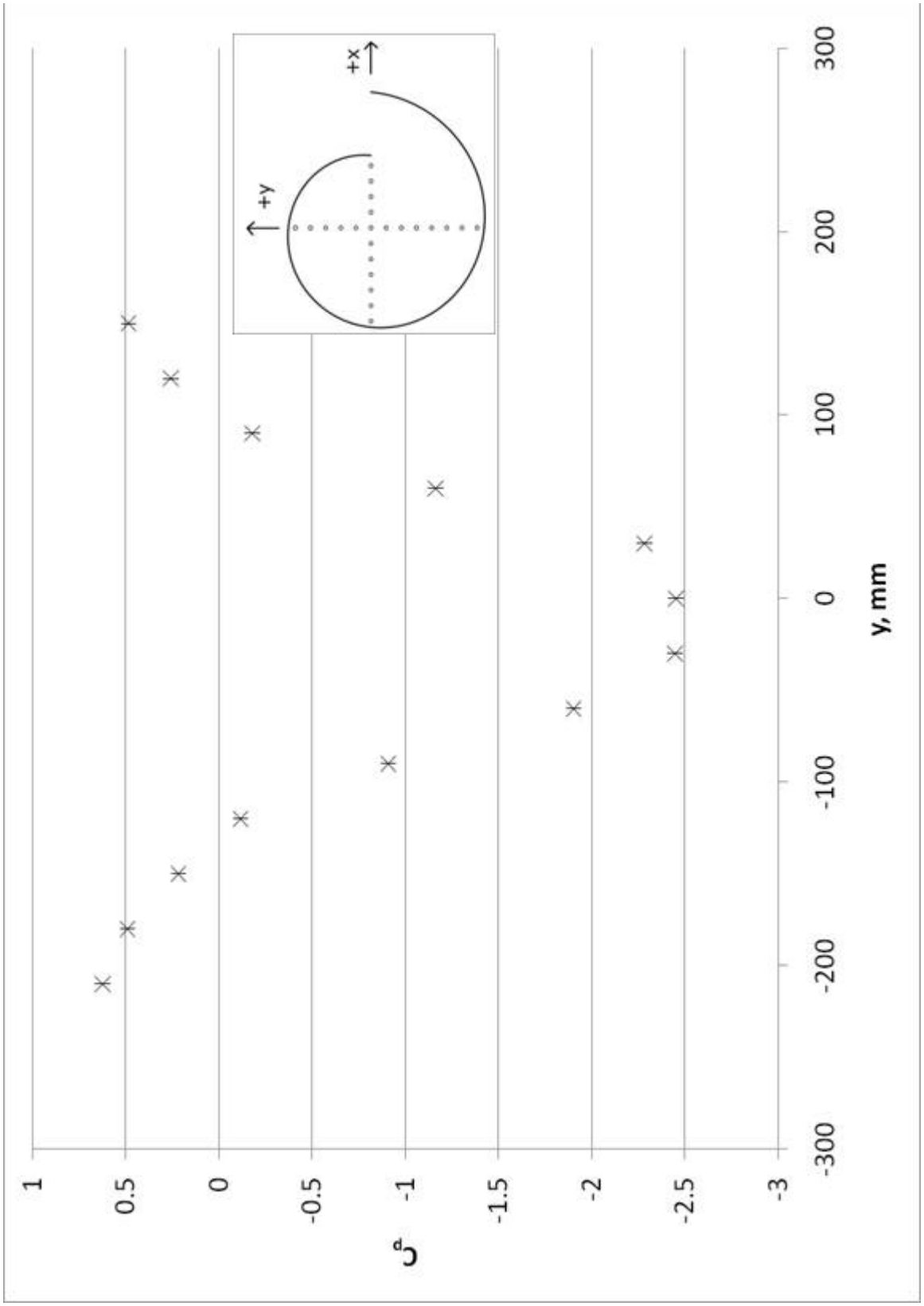

Figure 3.8 X-axis pressure coefficients, 36-in. model spiral chamber with flat floor, AABL wind tunnel, 5.7 m/s

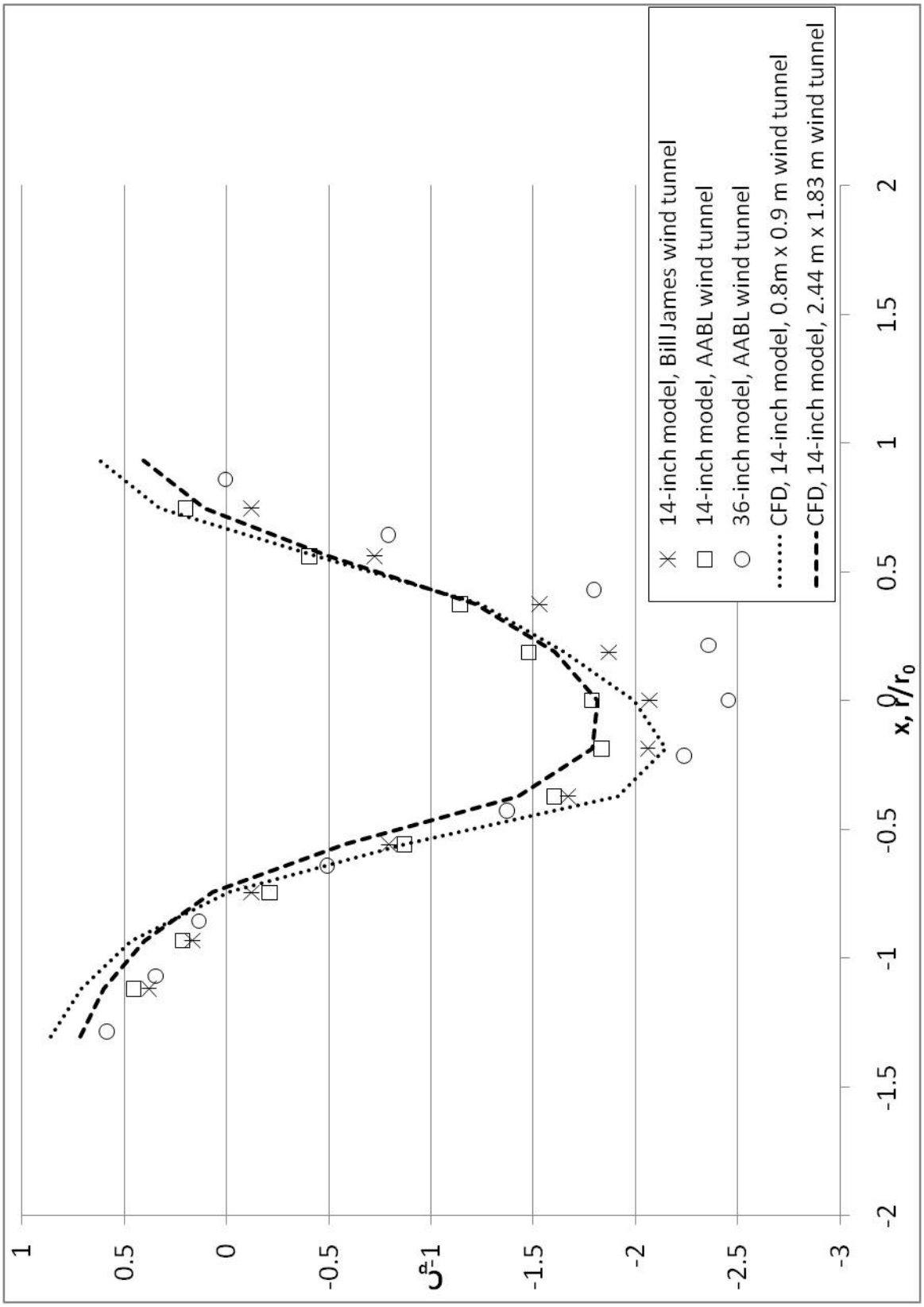

Figure 3.9 Y-axis pressure coefficients, comparison of various wind tunnel and CFD models

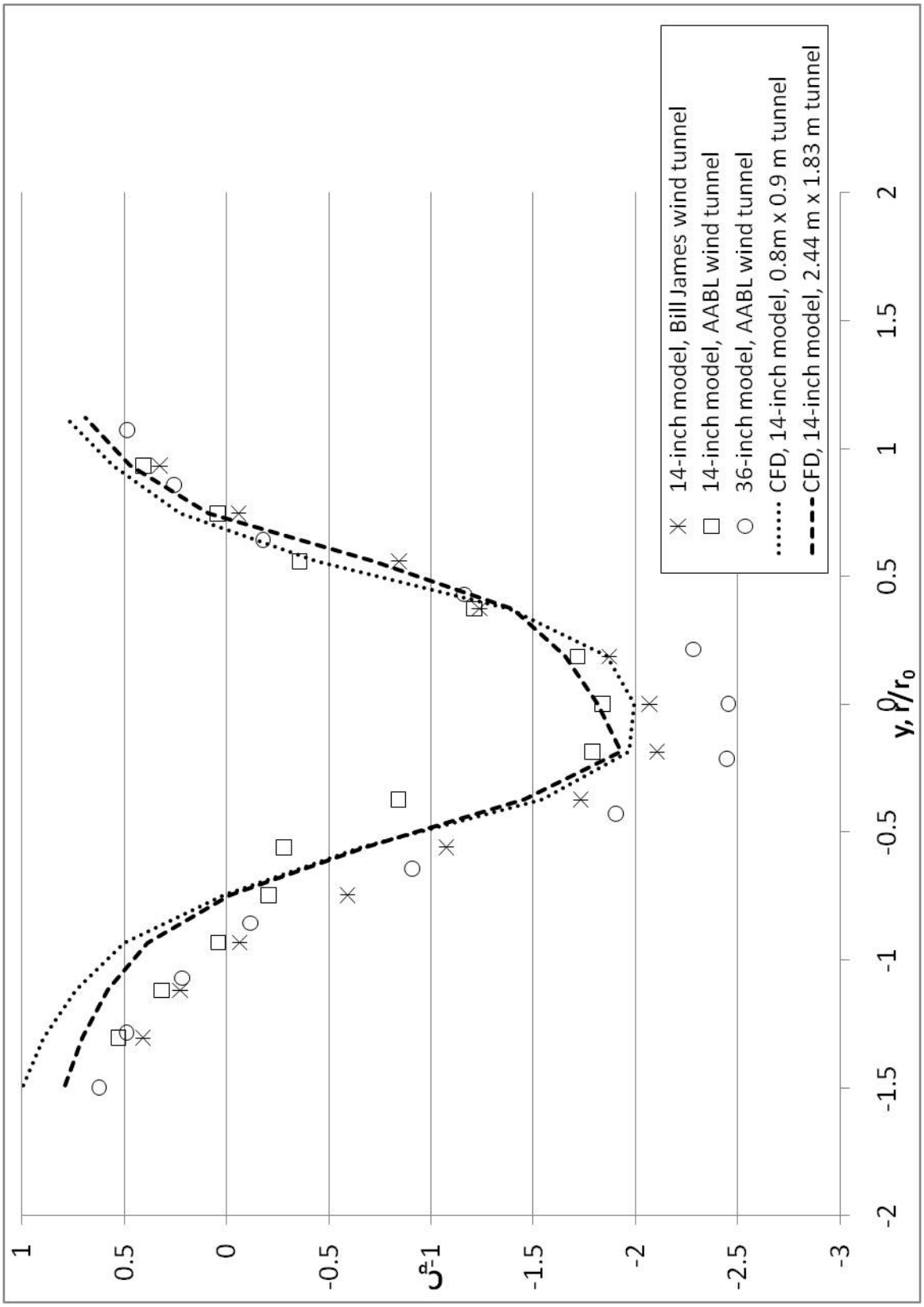

Figure 3.10 X-axis pressure coefficients, comparison of various wind tunnel and CFD models

does not stay at zero at all times. The in-plane velocities are greatest between the center and the walls, and smaller near the center and near the walls. This is the expected velocity distribution for a Rankine vortex. Figures 3.14 through 3.16 below show the numerical values of these velocities compared to a Rankine vortex.

Downstream and across-stream velocity vector planes are shown in Figure 3.13. This figure shows an updraft in the away from the core, and downflow near the core. This suggests that the vortex formed may be a multi-cell vortex, rather than a single-cell vortex. A multi-cell vortex may be detrimental for the current design for power extraction, as the fan may be placed in a region of adverse flow. Previous studies have focused on adding additional inflow to change the number of cells in the vortex.

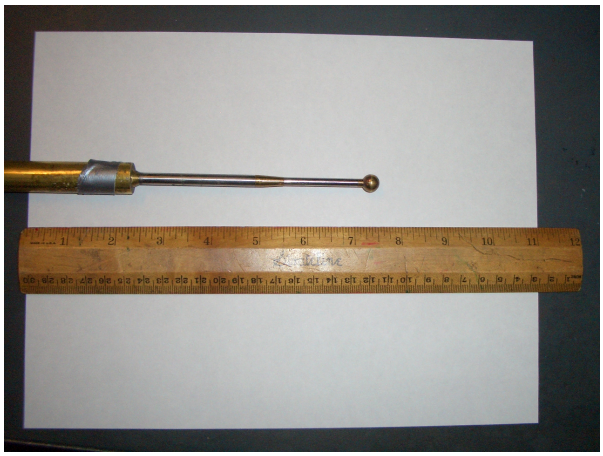

Figure 3.11 Omniprobe pitot-static probe

Horizontal in-plane velocities in the chamber are shown in Figures 3.14 through 3.16. The velocity distribution for a Rankine vortex (13) is shown with this velocity data. The velocities are shown for vertical heights of z/L=.222, .444, and .667, in both the across-stream (x=0) and downstream (y=0) directions. The positive-y direction is upstream, and the negative-y direction is downstream. The positive-x direction is towards the front inlet, and the negative-x direction is away from the front inlet.

The in-plane velocity plots all show Rankine vortex behavior, with the lowest velocities at the center and the edges. The difference between the lowest and highest velocities decreases as

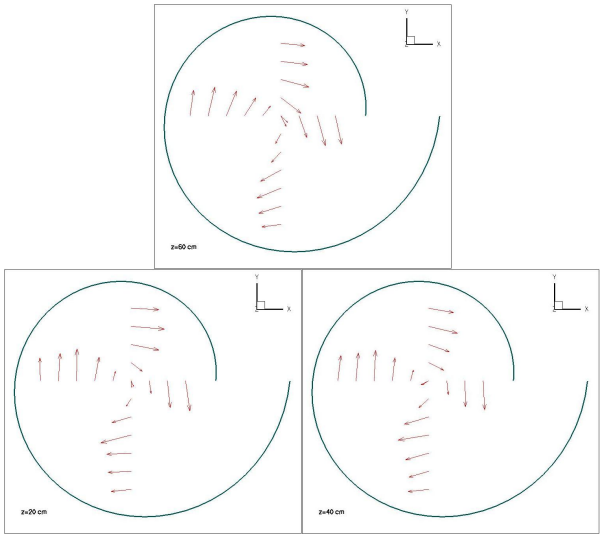

Figure 3.12 Top: Horizontal plane velocity vectors at z/L=.667
Bottom Left: Horizontal plane velocity vectors at z/L=.222
Bottom Right: Horizontal plane velocity vectors at z/L=.444

the height inside the chamber increases, showing a weakening of the Rankine vortex structure with height. Mohammad (11) studied the effect of changing the height-to-diameter ratio of the spiral chamber. He showed increasing pressure drops with increasing spiral chamber heights, showing that increasing the spiral chamber height (or increasing the height-to-diameter ratio) may result in a more powerful turbine.

Updraft velocities in the chamber are shown in Figures 3.17 through 3.19. The updraft velocity plots show adverse (downward) flow in the center, and sometimes also at the sides. This is consistent with a multi-cell vortex. Tesfamariam (14) shows the flow pattern for one-, two-, three-, four-, and five-cell vortices both with and without added radial inflow. Adding an appropriate amount of radial inflow can increase the updraft velocity in a vortex, and can change the number of vortex cells. Ide (10) did extensive work on using radial inflow to increase the power output of a TTWT and showed improvements, but his methods of adding inflow are somewhat impractical for a robust, low-cost design able to survive in the field.

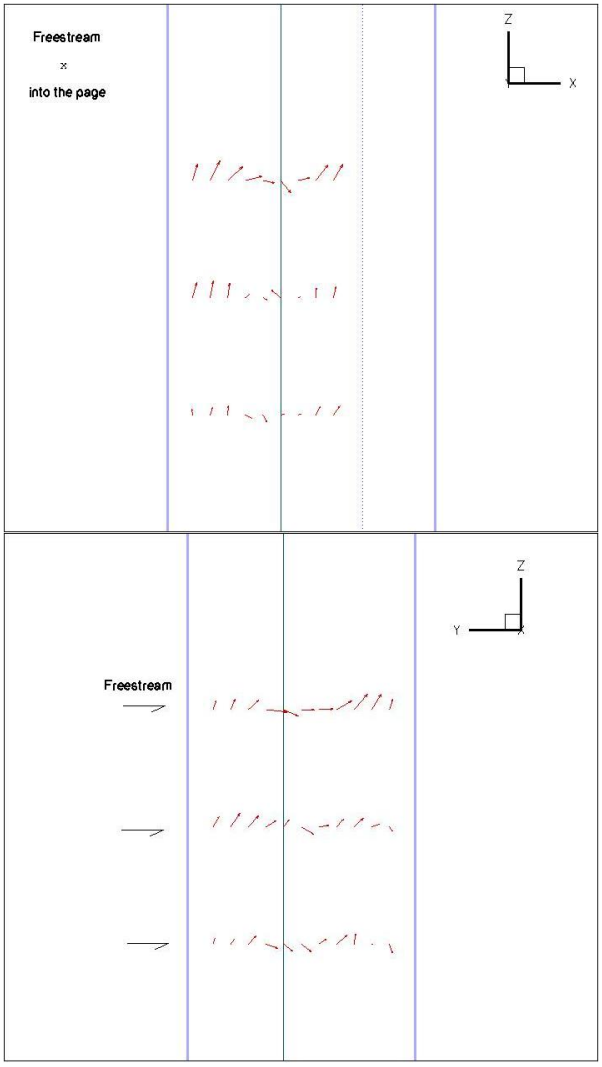

Figure 3.13 Top: Downstream velocity vectors
Bottom: Across-stream velocity vectors

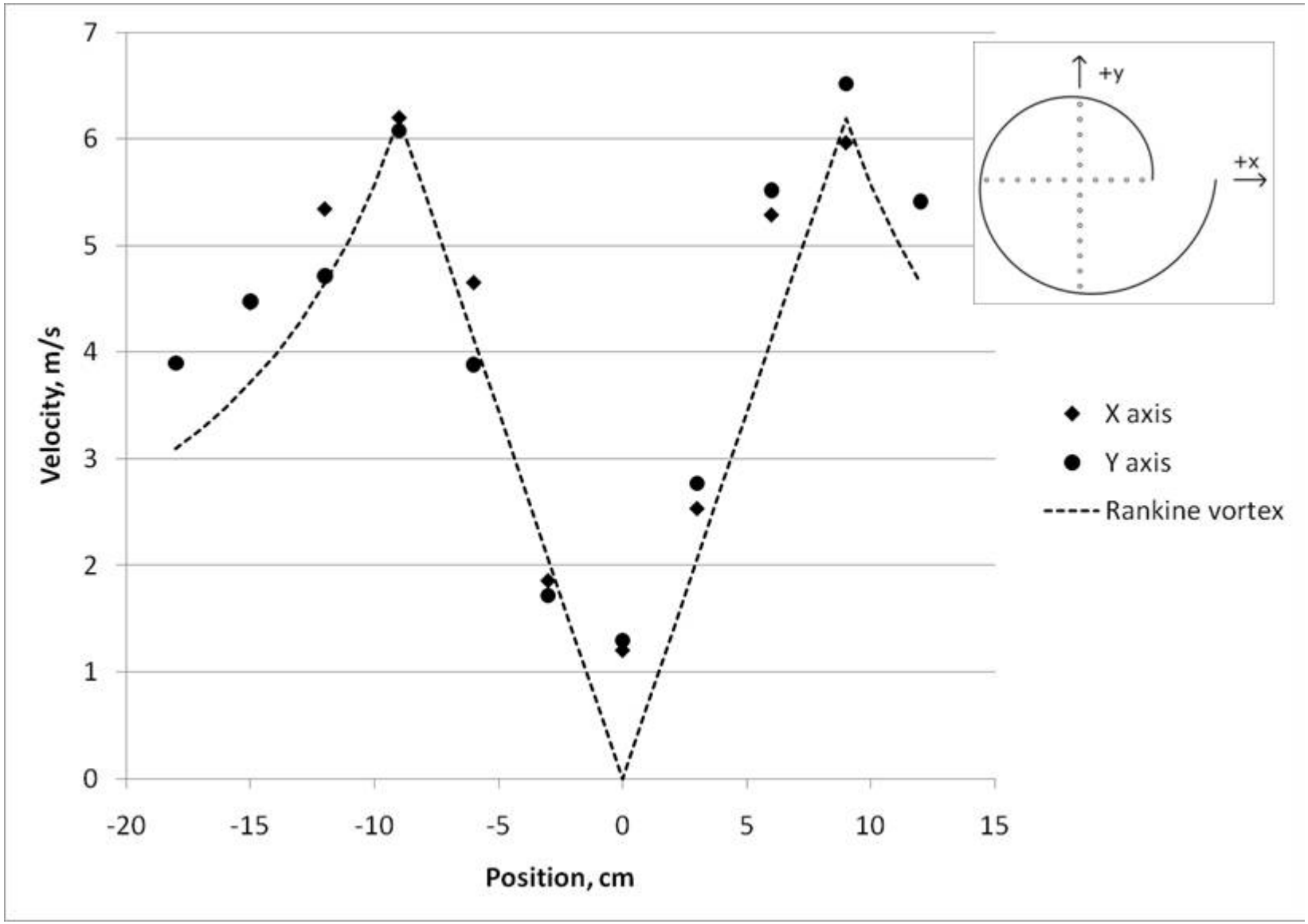

Figure 3.14 Horizontal plane velocity at z/L=.222, 36-in. model with large stagnation chamber, AABL wind tunnel, 5.7 m/s

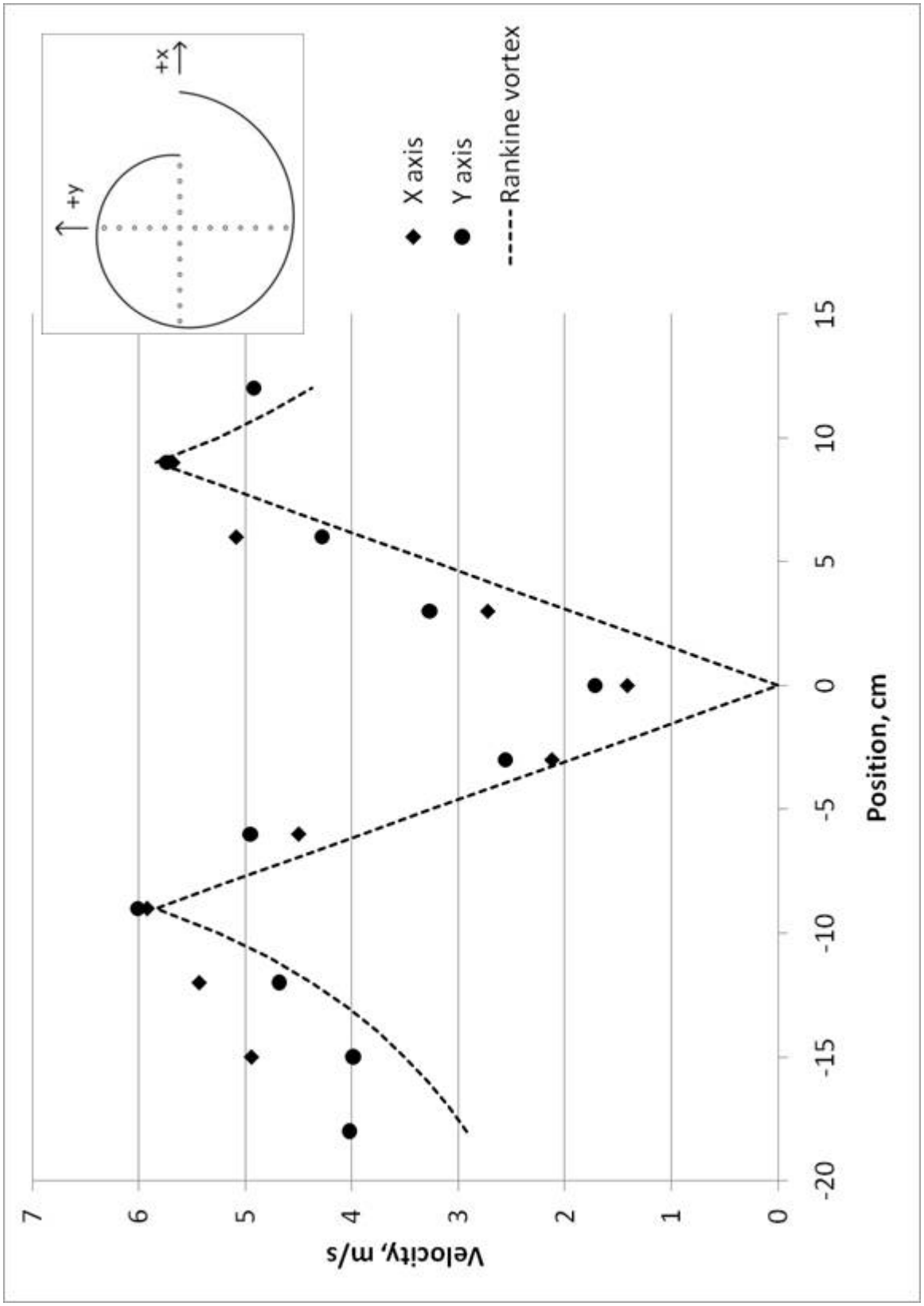

Figure 3.15 Horizontal plane velocity at z/L=.444, 36-in. model with large stagnation chamber, AABL wind tunnel, 5.7 m/s

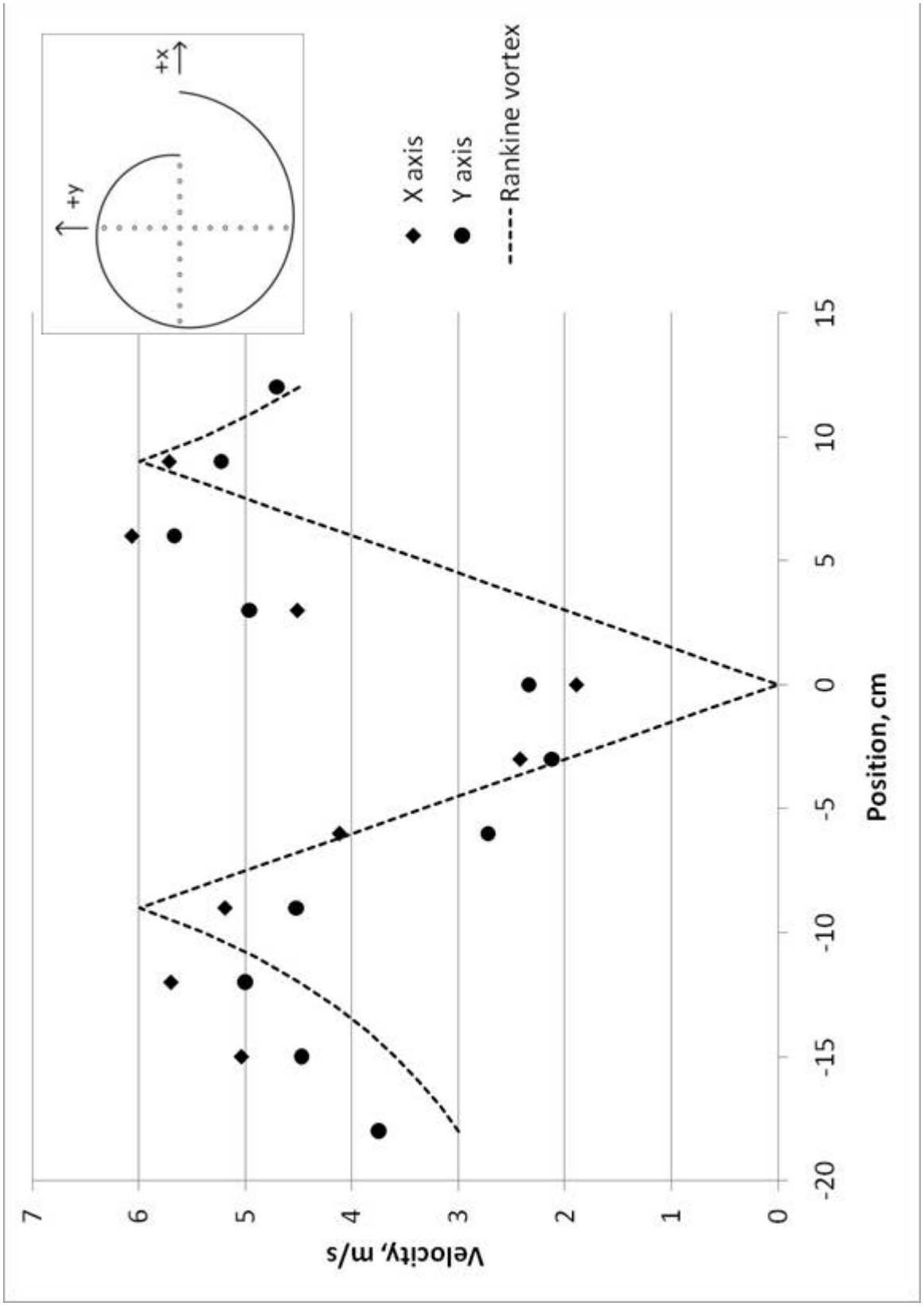

Figure 3.16 Horizontal plane velocity at z/L=.667, 36-in. model with large stagnation chamber, AABL wind tunnel, 5.7 m/s

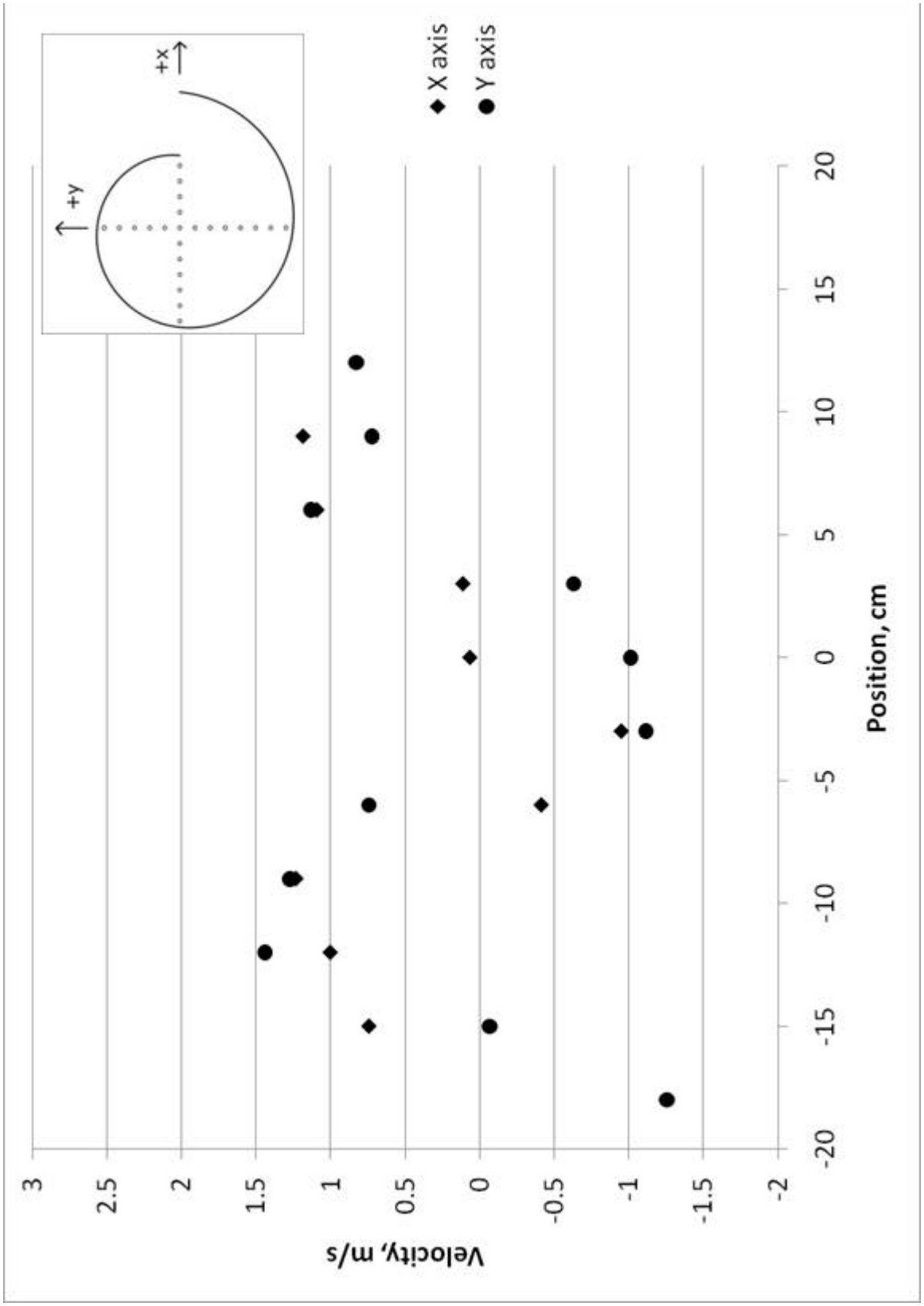

Figure 3.17 Updraft velocity at z/L=.222, 36-in. model with large stagnation chamber, AABL wind tunnel, 5.7 m/s

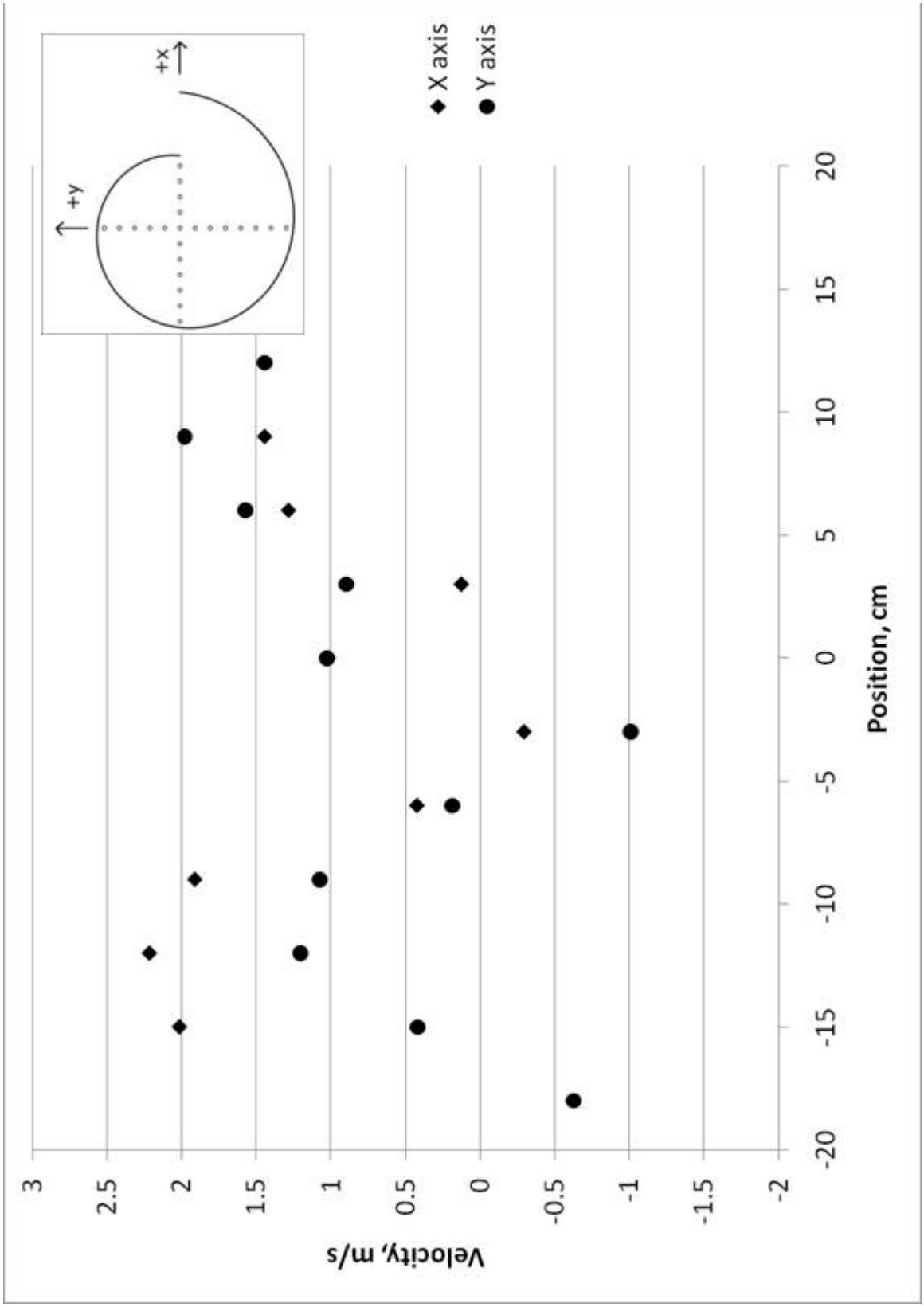

Figure 3.18 Updraft velocity at z/L=.444, 36-in. model with large stagnation chamber, AABL wind tunnel, 5.7 m/s

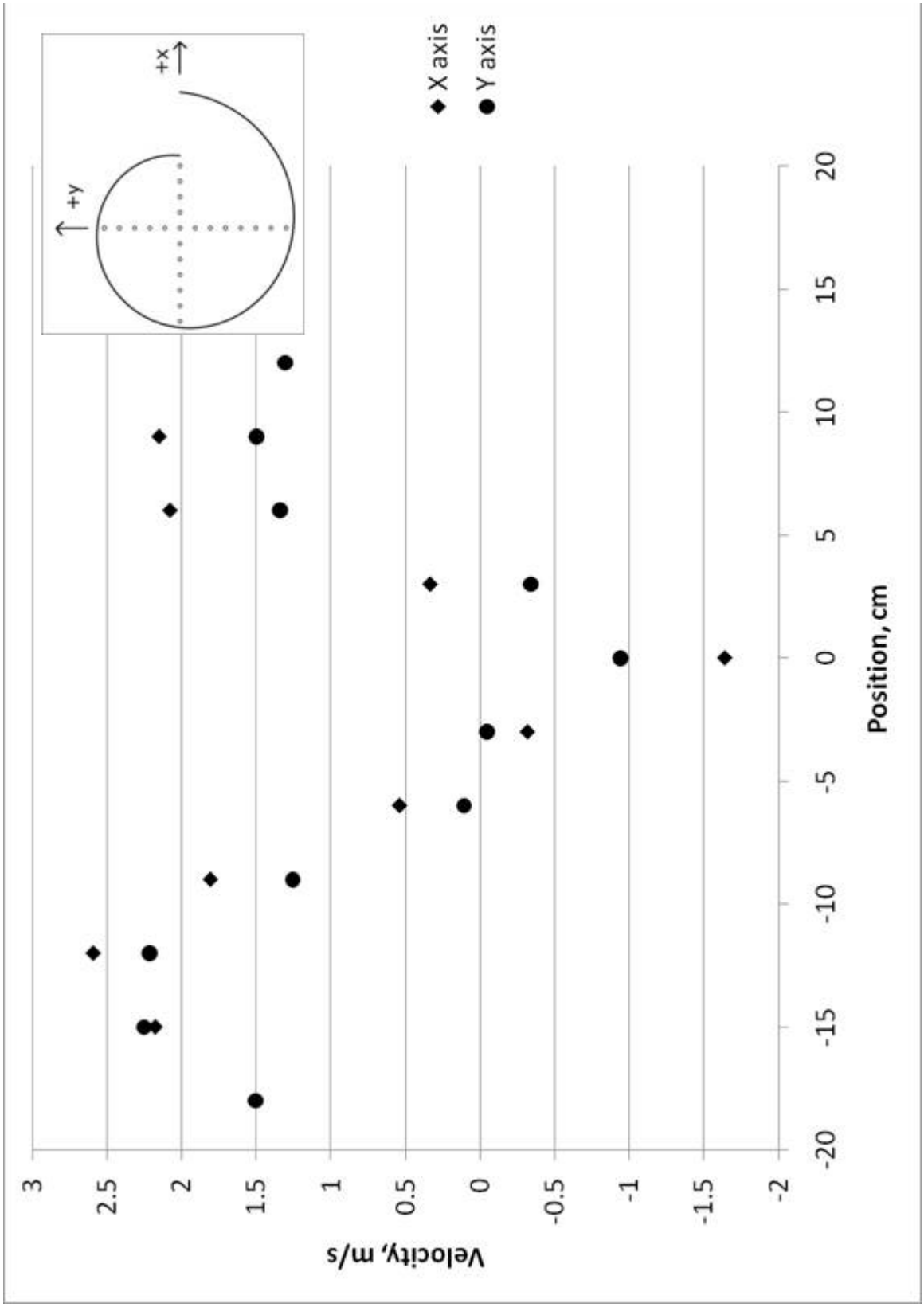

Figure 3.19 Updraft velocity at z/L=.667, 36-in. model with large stagnation chamber, AABL wind tunnel, 5.7 m/s

3.2.2 Center of Rotation

A logarithmic spiral is mathematicallly self-similar (changing r_0 has the same effect as rotating) and is centered on the origin. Logartihmic spiral occur often in nature, including in hurricanes. Some of the properties of logarithmic spirals may make them particularly suitable for the TTWT; consult a geometry text for more information. From its properties, it is not immediately evident where the center of rotation should be for a spiral chamber with this shape. Unlike other spiral shapes, the logarithmic spiral is always centered on the same point with respect to both rotation and scaling.

In order to determine the center of rotation, a grid of pressure taps with three centimeter separation was installed in the floor of the 36-in. spiral chamber. The locations of the grid points within the spiral are shown in Figure 3.20. Figure 3.21 shows the measured pressure coefficients on these grid points for a wind speed of 5.7 m/s. This figure shows that the lowest pressure location of the vortex, and thus the center of rotation, is located close to the origin, perhaps with a slight offset towards the negative-y direction.

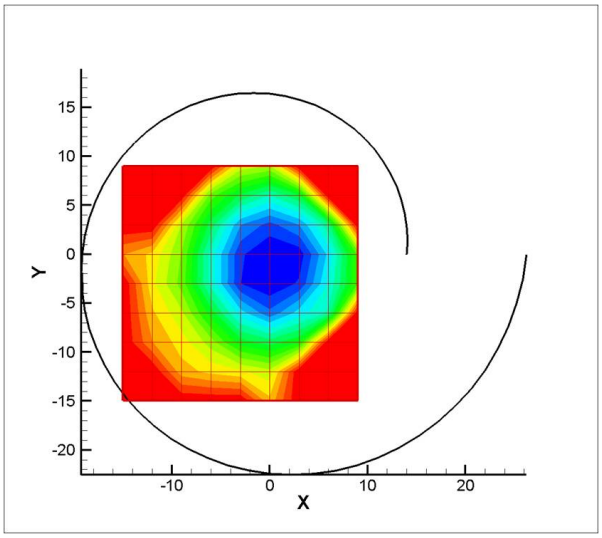

Figure 3.20 Coordinate system shown in relation to spiral geometry for center of rotation tests

A refinement of this grid was studied with pressure taps located 1 centimeter apart. Figure 3.22 shows the measured pressure coefficients near the origin at a wind speed of 5.7 m/s.

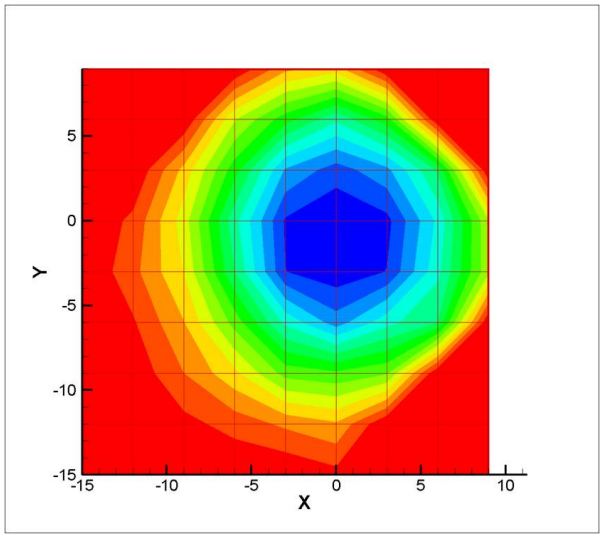

Figure 3.21 Pressure coefficient contours for 36-in. model with large stagnation chamber, AABL wind tunnel, 5.7 m/s

This figure shows that the center of rotation is within one centimeter of the origin. The fan or other extraction device is to be installed in the floor of the spiral chamber at the center of the vortex. The floor pressure measurements show that centering the fan at the origin of the coordinate system will place the fan quite close to the center of the vortex.

3.2.3 Lids

The velocity vectors in the spiral chamber, shown above, suggest that much of the rotating air is escaping out of the top of the spiral chamber. At this point most of the velocity is still in the horizontal plane, so the rotation of the flow is more important than the upward flow.

The TTWT concept relies on a rotating outer mass of air to generate a region of negative pressure. In order to contain the rotating mass of air to allow the core air to develop fully, a variety of lid sizes were tested. Each lid blocked the top of the spiral chamber, with a circular hole centered on the origin of the spiral geometry. The pressure coefficient was measured across the spiral chamber floor for lids with holes ranging from 2 cm to 12 cm in radius. For comparison, r_0 (the initial radius of the spiral) was 14 cm.

Figures 3.23 and 3.24 show the measured floor pressure coefficients for various lid hole

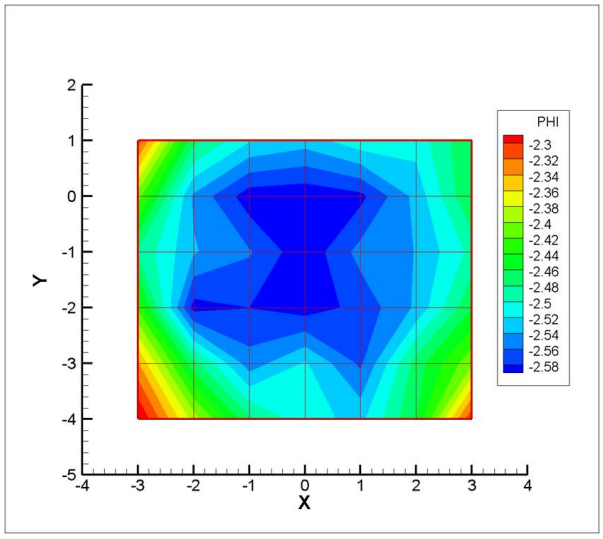

Figure 3.22 Refined pressure coefficient contours for 36-in. model with large stagnation chamber, AABL wind tunnel, 5.7 m/s

sizes. The pressure coefficient curve for the case with no lid is also shown for comparison. The pressure coefficient drop for the smallest radii holes was negligible, consistent with a closed chamber with insufficient ventilation. Increasing hole sizes generally led to increased pressure coefficient drops. Containing some of the outermost flow helps to strengthen the vortex structure, but confining the exit area too much chokes the flow and does not allow sufficient mass flow through the system.

Figure 3.24 shows that the lowest pressure drop along the cross-stream (x-axis) direction does not always occur at the origin, which was shown above to be roughly (within 1 cm) the natural center of rotation for the vortex. This suggests that the vortex core is migrating due to interaction with the lid.

The best pressure coefficient drop, to -4, is an improvement over the pressure drop to -2.5 in the open case. The pressure coefficient curve is low only in a narrow range for the lid cases, however the fan or extraction device would not be as large as the entire spiral chamber floor, so the pressure coefficient curve is low in the area where the fan would be placed.

Although the lids tested showed an improved pressure drop in the spiral chamber, the lids did not show improvement when used in the complete TTWT system, and thus other

modifications to the top of the spiral chamber were made.

Additional work should be done on other lid designs, including different shapes or placements for the hole to accommodate the center of rotation migration observed.

3.2.4 Stagnation Chamber

The TTWT was mounted on top of a stagnation chamber similar to the chamber used by Minachi (6). Three different sizes of floor holes were tested, 2.5 cm, 5 cm, and 12 cm. For comparison r_0 was 14 cm. The holes were thus $0.18 * r_0$, $0.36 * r_0$, and $0.86 * r_0$.

In addition to the flow through the TTWT due to the vortex, a certain amount of flow is expected due to the suction effect from the air passing over the spiral chamber and the forced air flow exhausting up from the stagnation chamber. The combination of these two effects is sometimes called the "chimney effect" because it is the amount of flow that would occur in a closed cylinder above a stagnation chamber. To examine the efficacy of the spiral chamber on TTWT performance compared to the chimney effect, all hole sizes were tested with the front air intake of the spiral both open and blocked off.

A pitot-static tube was inserted into the hole with the static ports in the plane of the spiral chamber floor. Pressure coefficients across the hole were measured simultaneously with floor pressure coefficients. The pitot-static tube was also used to measure the flow velocity. Figure 3.25 shows the placement of the pitot-static tube for these tests.

Figures 3.26 through 3.28 show the velocity increase across the hole for various hole sizes with the front intake both open and blocked. The smallest hole size ($0.1786 * r_0$) yielded the largest velocity increase, more than doubling the velocity of the freestream air. The middle hole size ($0.357 * r_0$) also showed improvement over the freestream velocity, but the improvement was similar for both the open intake, corresponding to the full vortex-assisted TTWT, and the closed intake, showing just the chimney effect. The largest hole ($0.86 * r_0$) showed a decrease in performance, slowing the air below the freestream velocity. For this case the chimney effect still accelerated the air, but not as much as with smaller holes. This suggests that the vortex is interacting with the air in the stagnation chamber and there is not enough spiral chamber

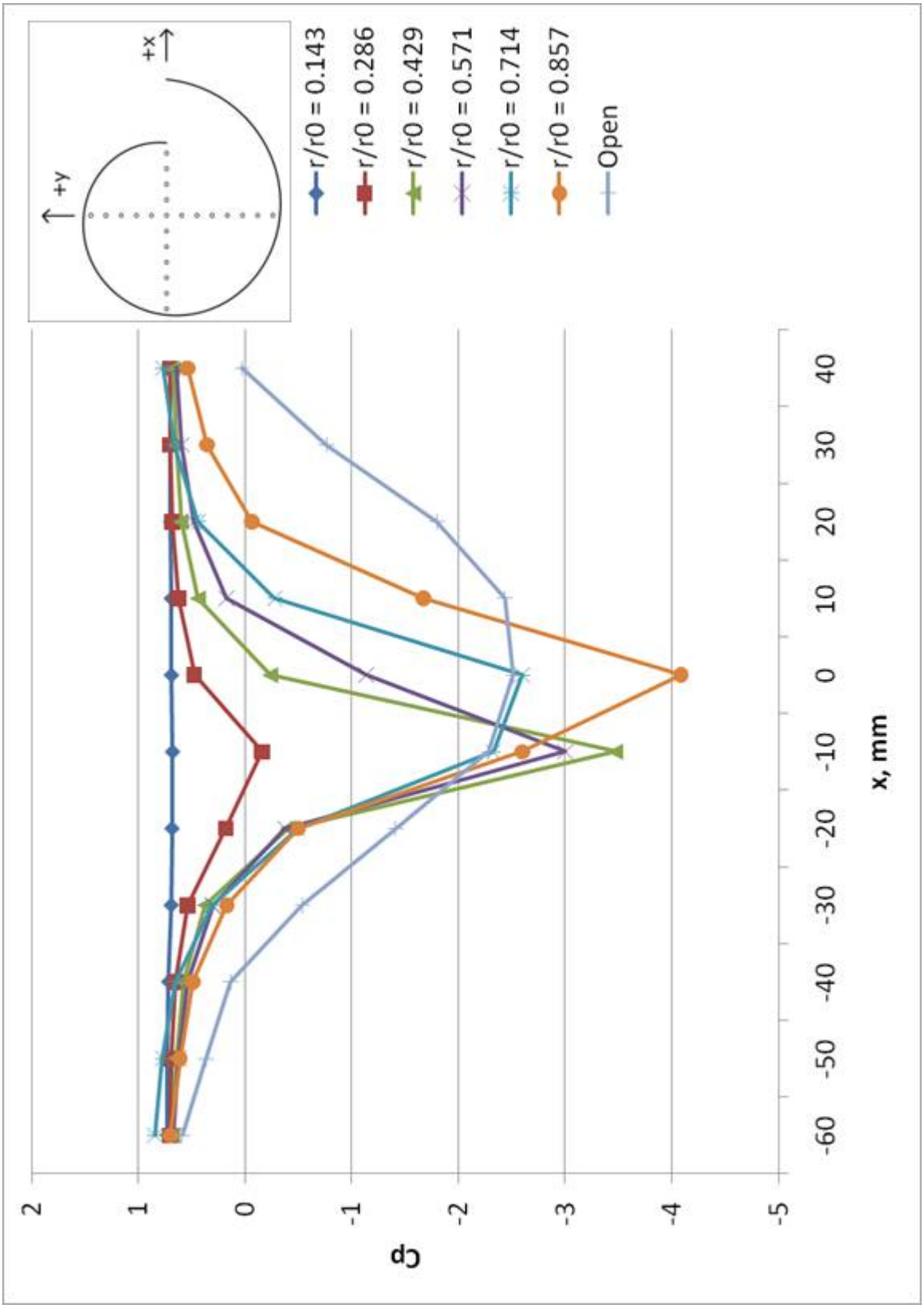

Figure 3.23 X-axis pressure coefficients, 36-in. model with large stagnation chamber, various lids on spiral chamber, AABL wind tunnel, 5.7 m/s

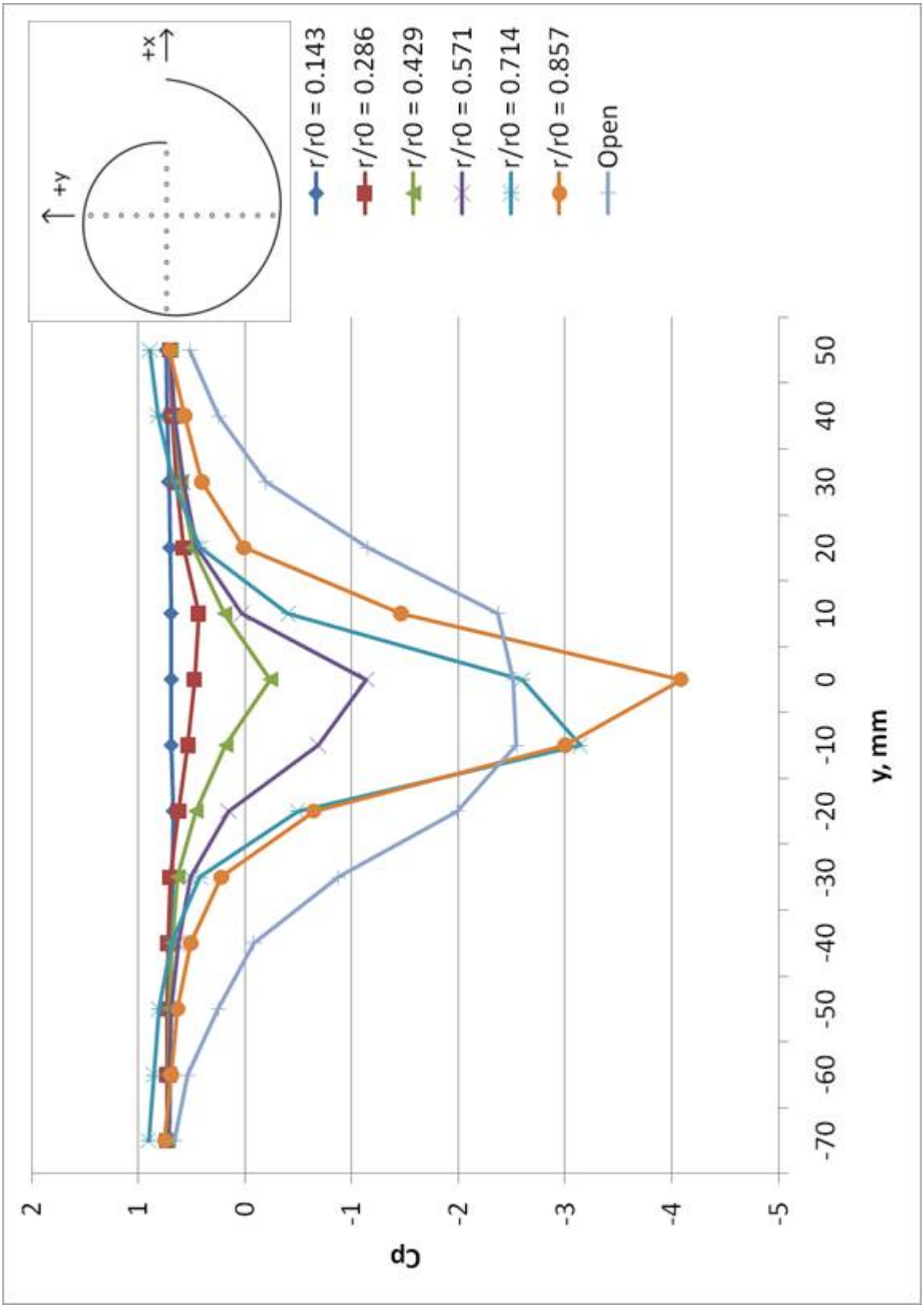

Figure 3.24 Y-axis pressure coefficients, 36-in. model with large stagnation chamber, various lids on spiral chamber, AABL wind tunnel, 5.7 m/s

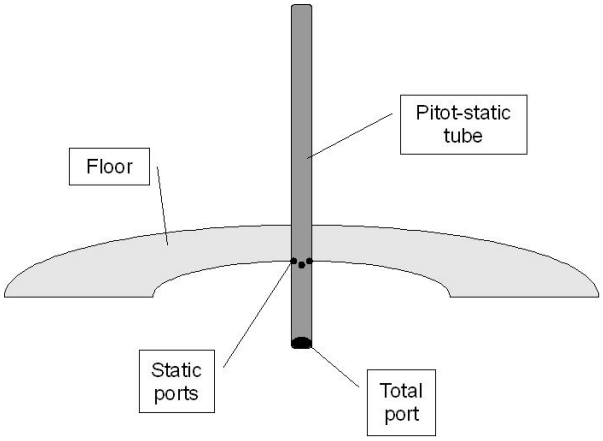

Figure 3.25 Schematic showing placement of pitot-static tube for measurements of pressure coefficients and velocities in TTWT throat

floor area to contain the rotating outer mass of air.

Figures 3.29 through 3.31 show the pressure coefficients across the spiral chamber floor and across the hole. As expected, the pressure coefficient data shows the same trends as the velocity data. For the largest hole size, the pressure coefficients show variability both downstream and across-stream for the chimney case but not for the vortex flow case. This suggests an interaction with the flow coming through the stagnation chamber.

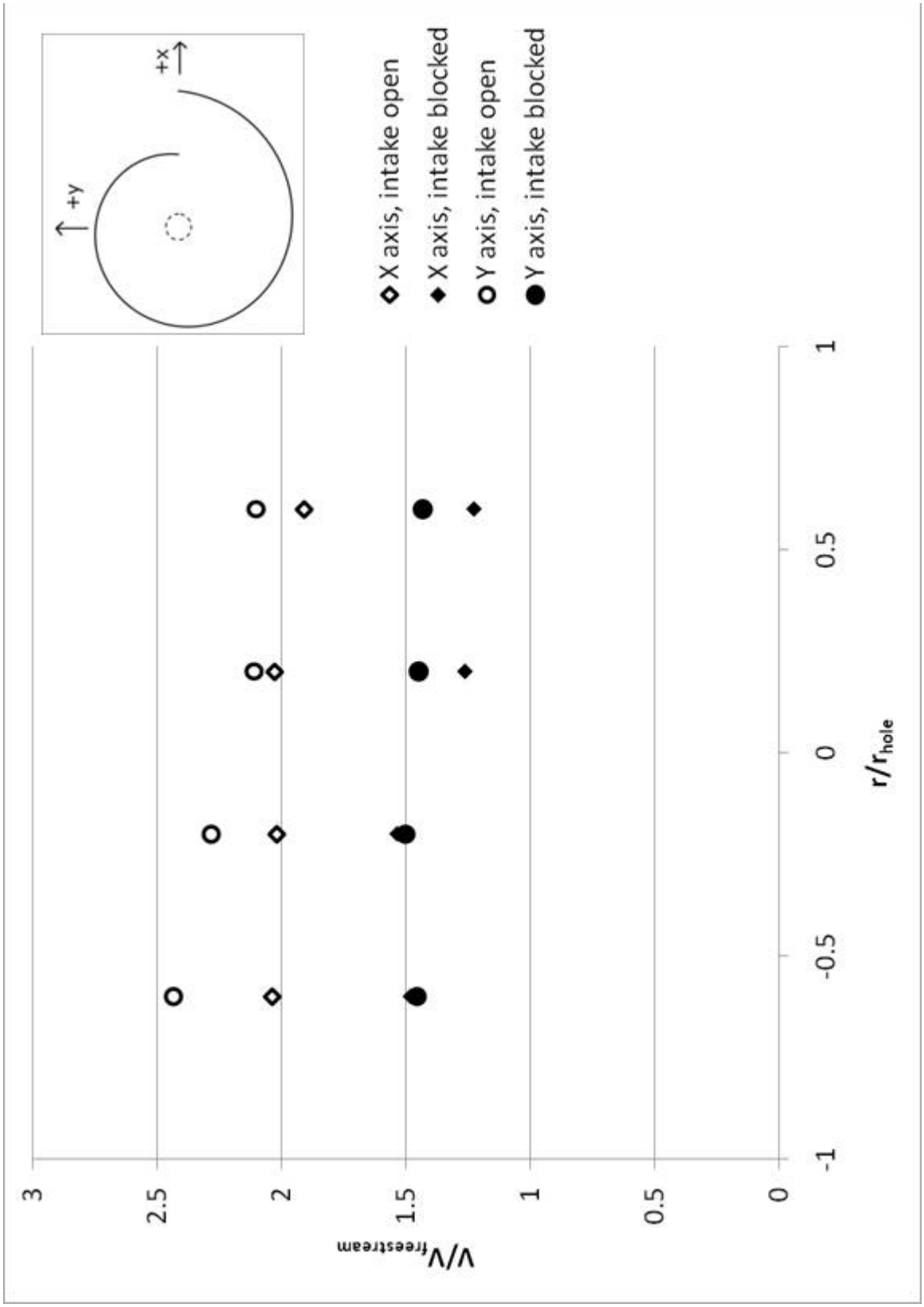

Figure 3.26 Velocity increase in throat, hole size and location shown ($r = 0.1786 * r_0$)

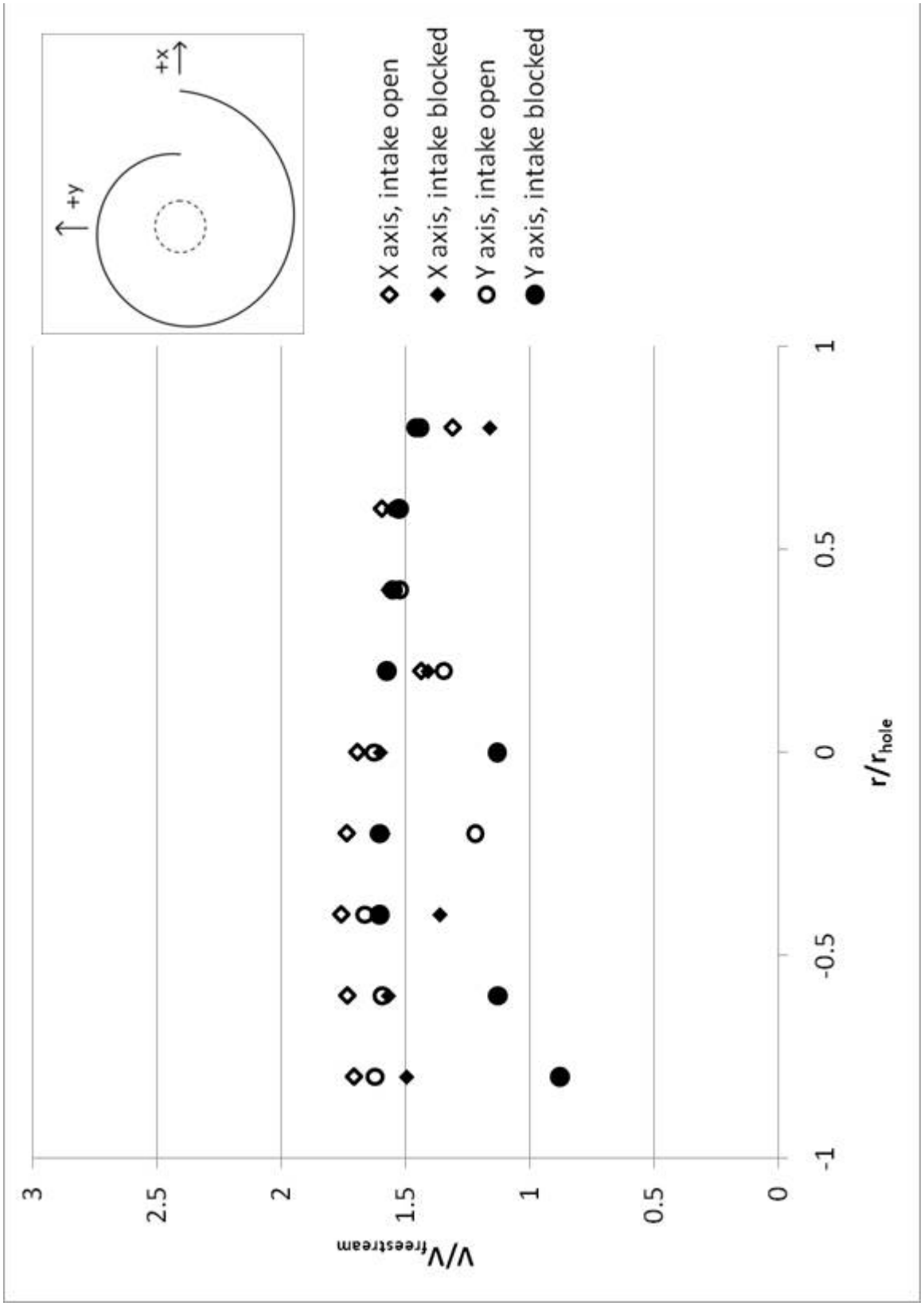

Figure 3.27 Velocity increase in throat, hole size and location shown ($r = 0.357 * r_0$)

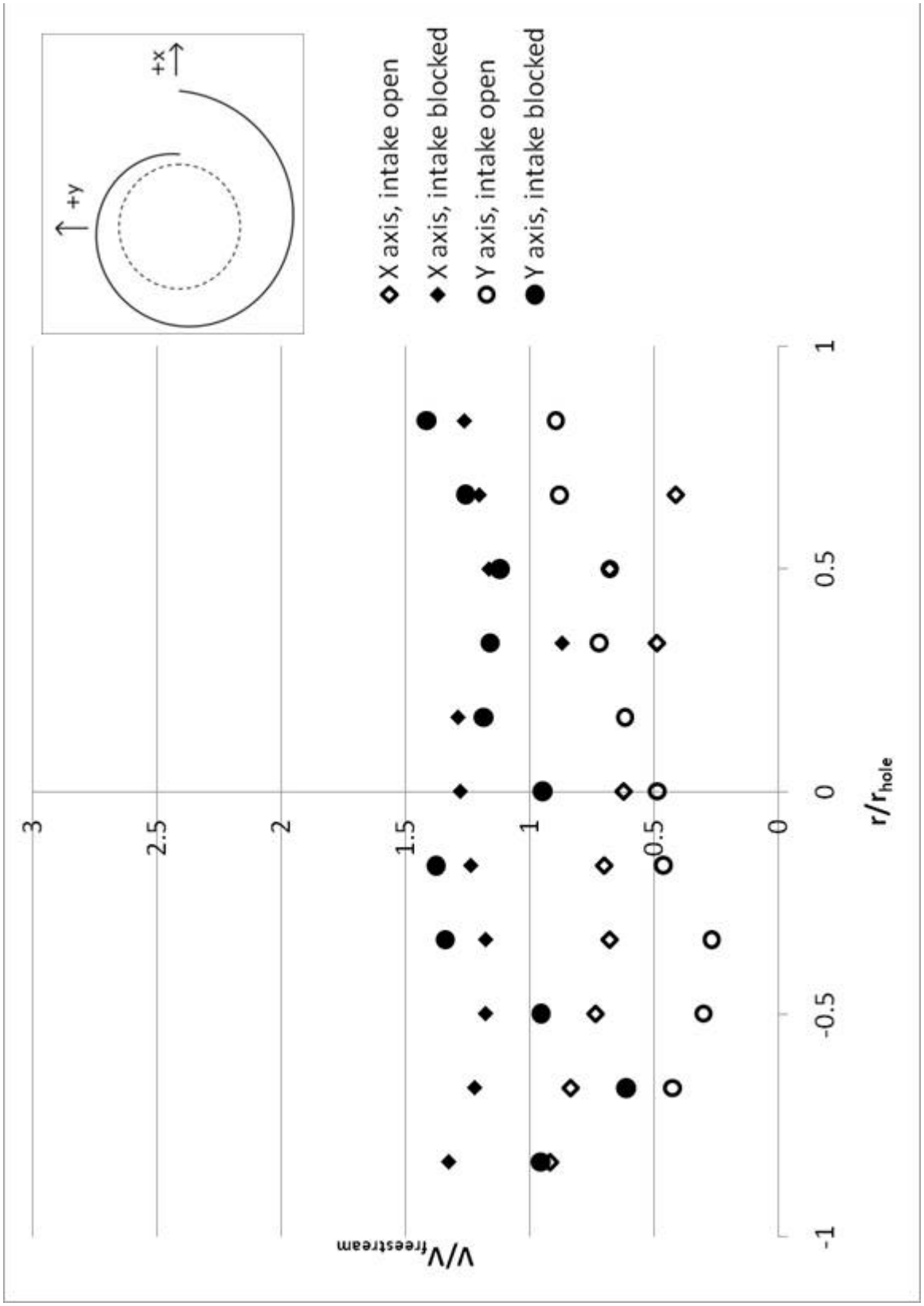

Figure 3.28 Velocity increase in throat, hole size and location shown ($r = 0.857 * r_0$)

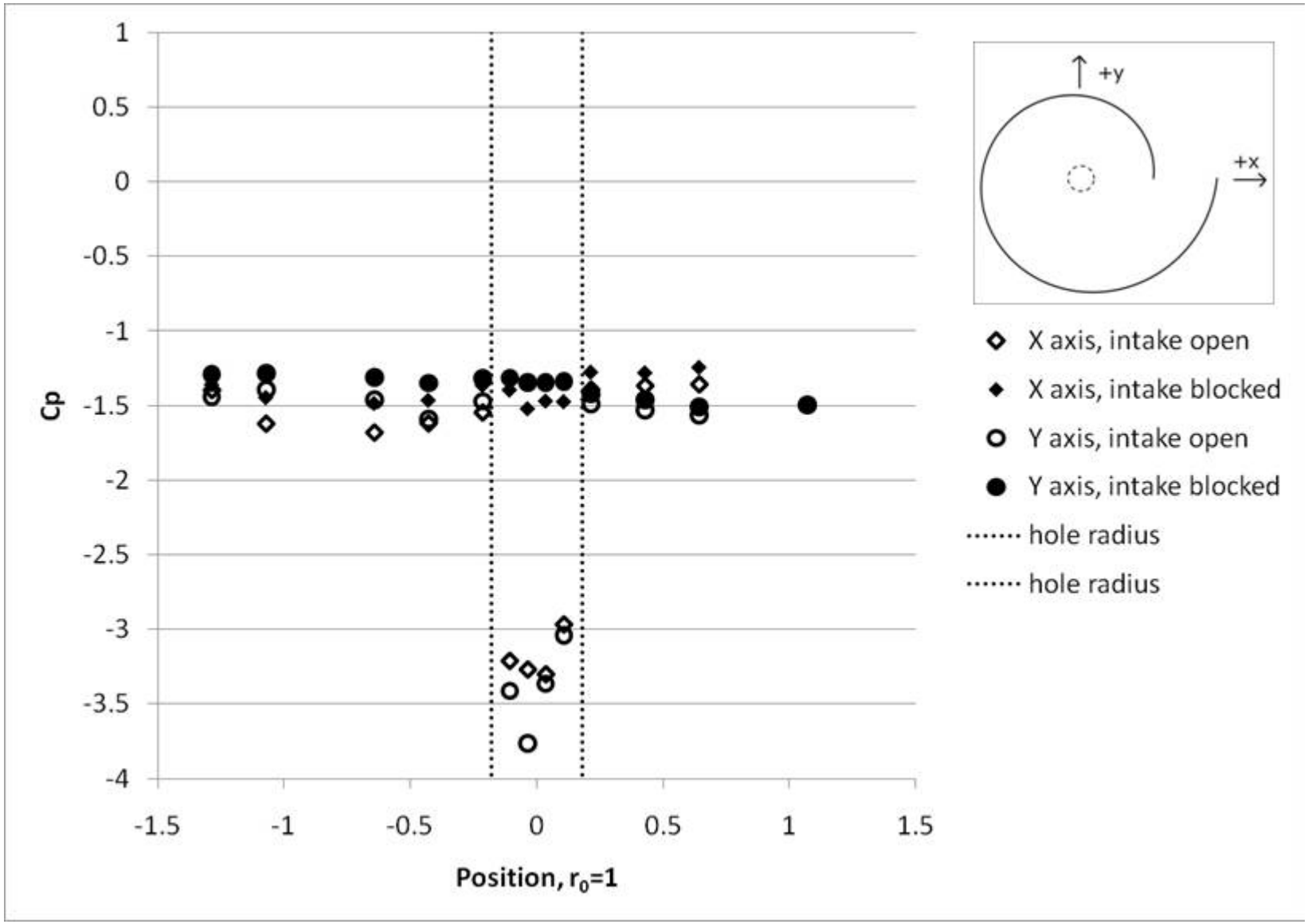

Figure 3.29 Pressure coefficient across floor and throat, hole size and location shown ($r = 0.1786 * r_0$)

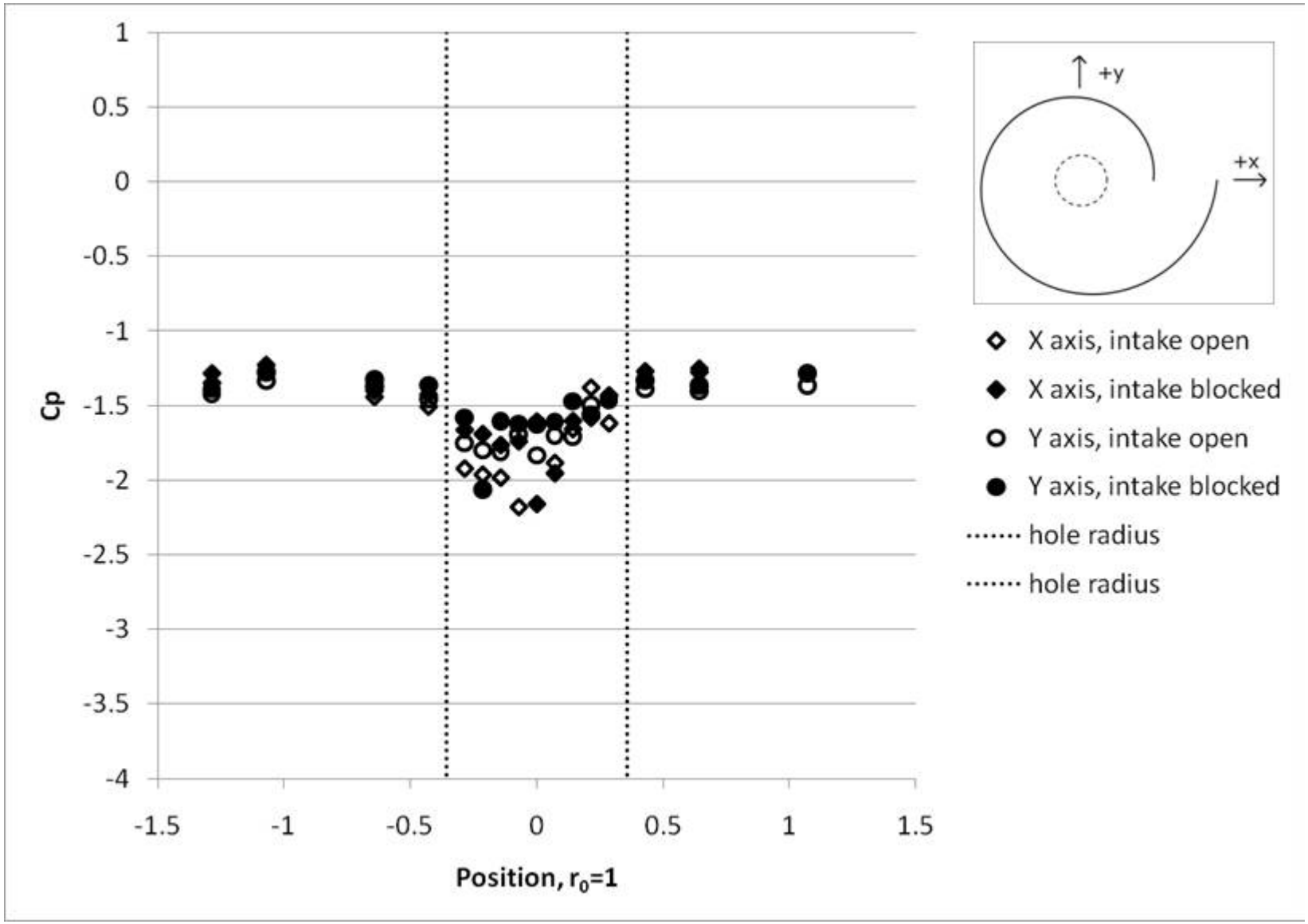

Figure 3.30 Pressure coefficient across floor and throat, hole size and location shown ($r = 0.357 * r_0$)

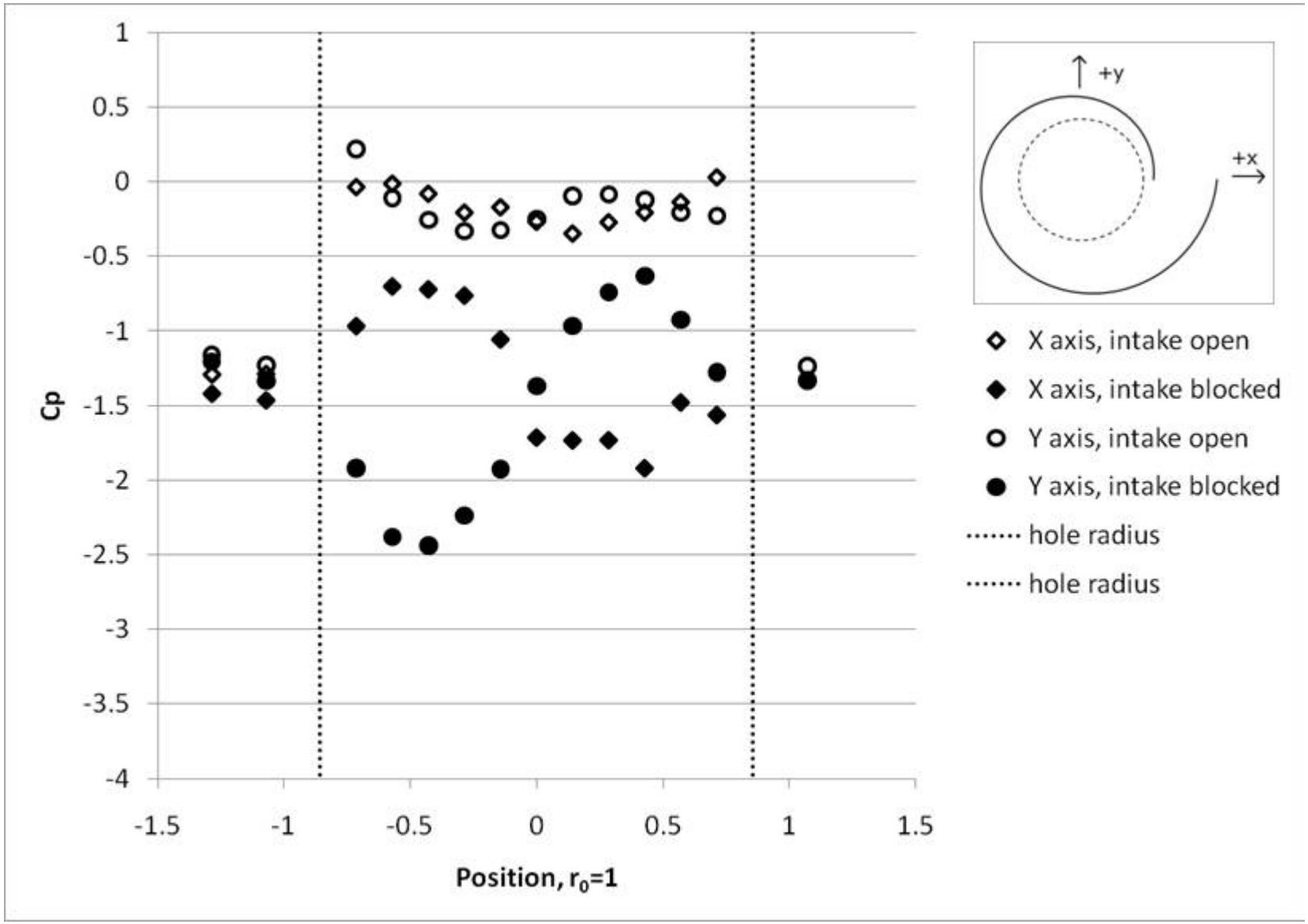

Figure 3.31 Pressure coefficient across floor and throat, hole size and location shown ($r = 0.857 * r_0$)

3.3 Best Improvements

The best combination of improvements were a ramp at the inlet floor, blockage of the top sixth of the spiral inlet, and an extension of the front of the spiral chamber wall. A small stagnation chamber with quarter-pipe inserts is used. The 36-in. spiral chamber is used with the modifications listed.

The power delivered by the best combination of improvements was measured with a modified small desk fan. The fan was taken out of the its housing and placed in the throat of the TTWT. Figure 3.32 shows the fan mounted in the TTWT. A power resistor was placed in a circuit with the fan leads to simulate loading, and the current and voltage in the circuit were measured to derive power output. Power output was measured over a range of freestream velocities for the fan in the TTWT throat. Power output was also measured for the fan alone in the freestream.

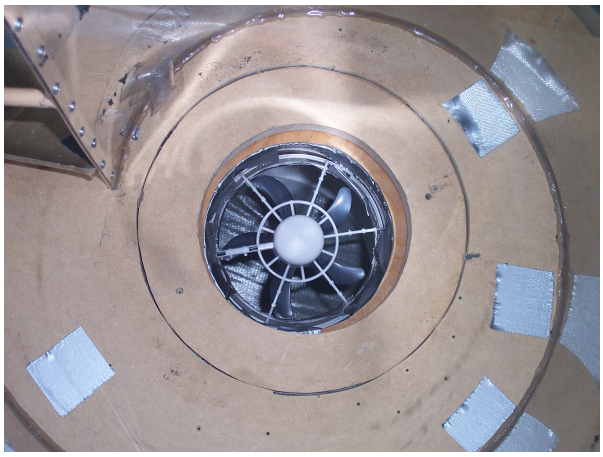

Figure 3.32 Fan installed in throat of TTWT
Model fabricated by Bill McClintic, modifications by J. Pierce Scarlett, photo courtesy J. Pierce Scarlett

Power measurements from this fan allow comparisons of the increase in power delivered by the fan in the TTWT throat compared to the same fan in the freestream. Figure 3.33 shows the power delivered to the fan alone in the freestream and the power delivered to the fan in the TTWT throat.

This power measurement can also be used to arrive at a rough "effective velocity," the

velocity that freestream air would be at to generate the measured power. For the best TTWT configuration tested, the effective velocity is greater than 1.4 times the freestream velocity.

To demonstrate the power potentially available with the TTWT, the power curve for a representative small wind turbine available today, the Air-X (15), was found. Based on the velocity increase factor, an appropriately scaled TTWT with this turbine in its throat would generate more power than this turbine alone. Figure 3.34 shows the power curve for the Air-X turbine by itself, and the extrapolated power curve if it were placed in an appropriately sized TTWT.

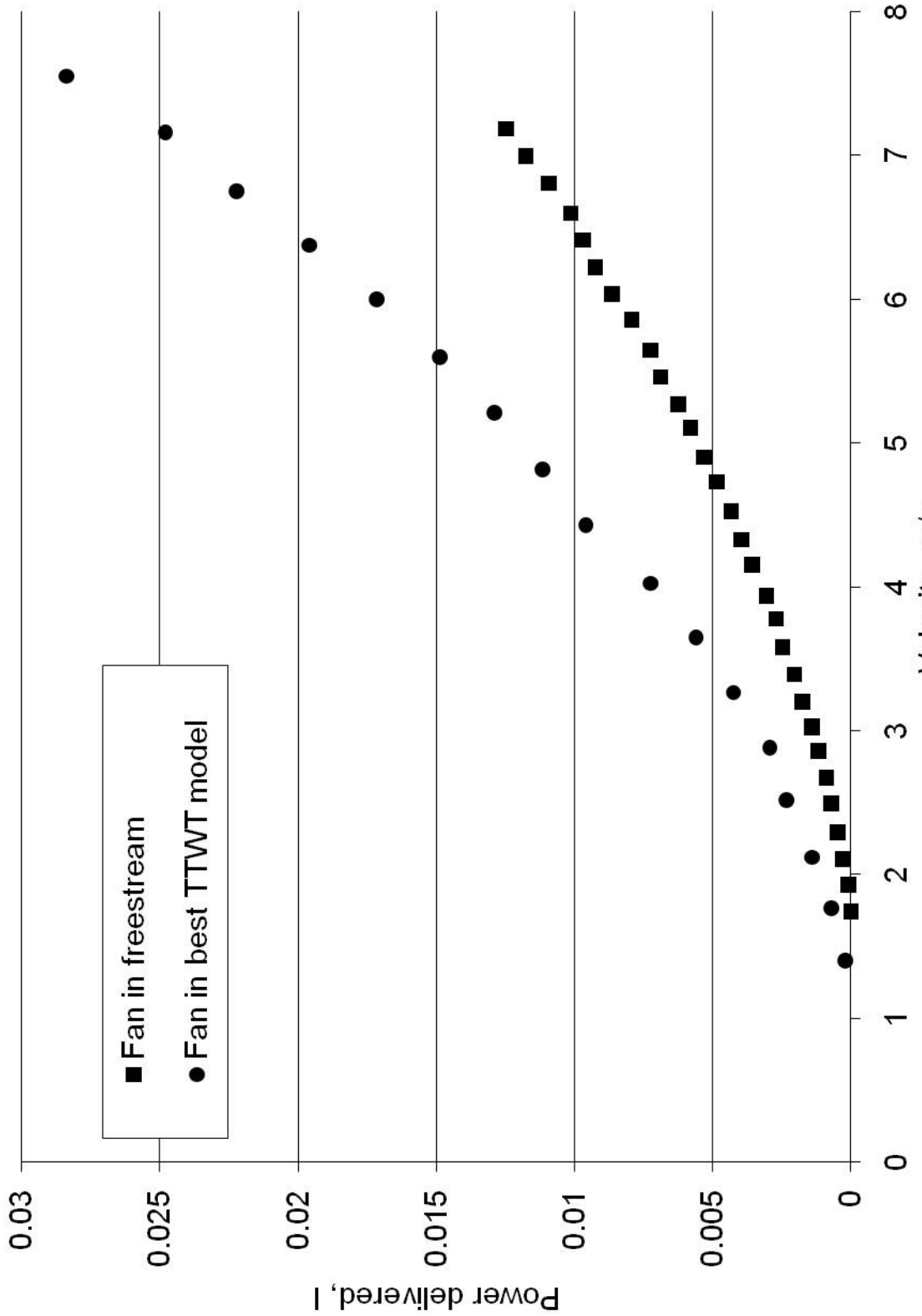

Figure 3.33 Power delivered by fan in TTWT and in freestream, AABL Wind Tunnel, various freestream velocities

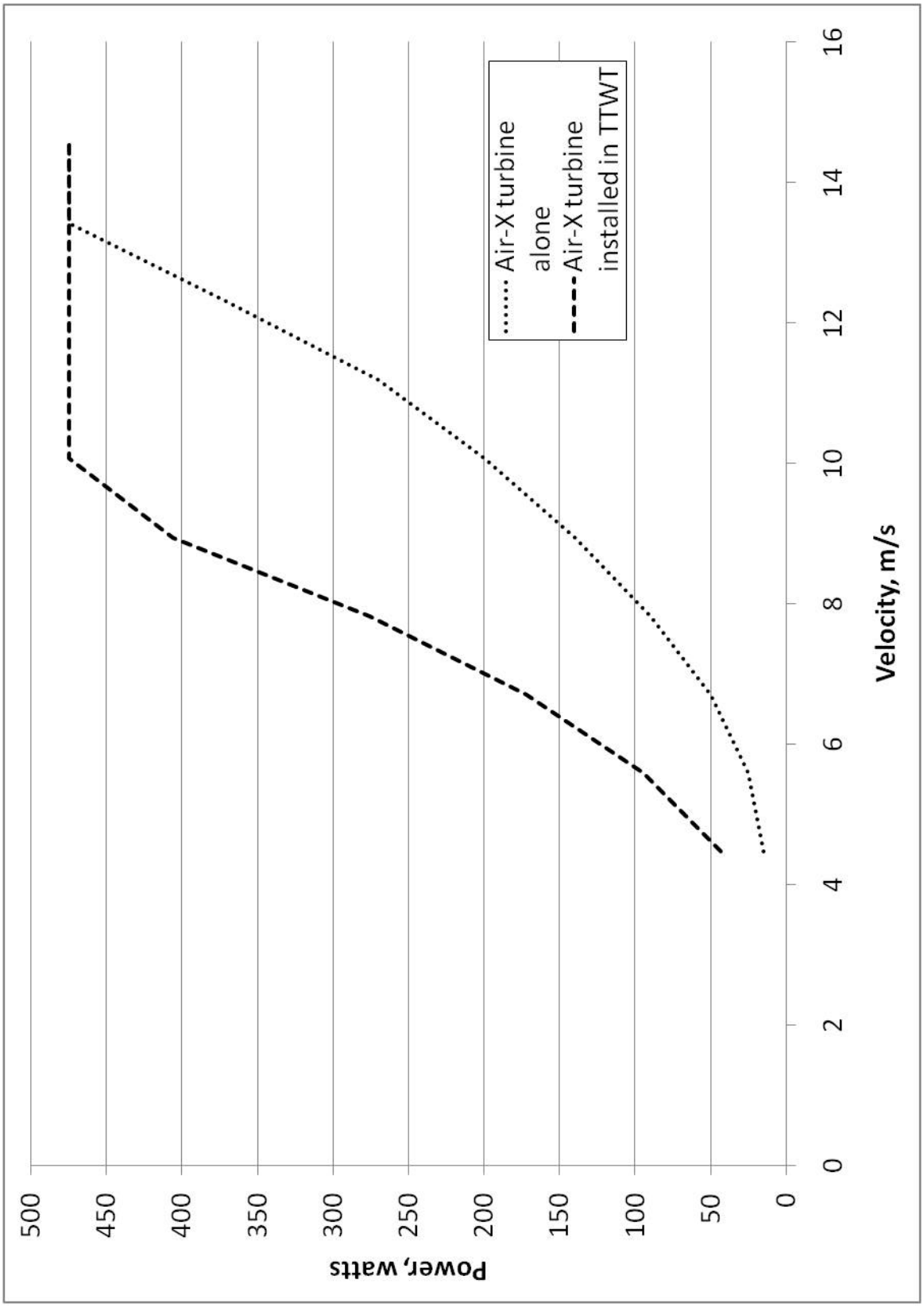

Figure 3.34 Power curve for Air-X turbine in freestream, and extrapolated power curve for Air-X turbine in TTWT throat

CHAPTER 4. CONCLUSIONS AND RECOMMENDATIONS

4.1 Introduction

The results from this study show that the TTWT can be improved to make a viable niche product for the energy market. Many of the improvements discovered did not derive directly from obvious theoretical considerations, but rather from exhaustive trials of many potentially helpful modifications. Continued work will very likely discover additional modifications to further increase performance, and much work remains to be done on identifying an optimal fan or extraction device for the throat.

Modern experimental techniques now exist to quantify flow properties that were unavailable in the 1980s, when the most recent work had been done. Computational fluid dynamics software is now able to provide high-fidelity simulations in a reasonable amount of time. The WiST laboratory at Iowa State is equipped to simulate wind gusts and turbulent inflow, more representative of the environment in which the TTWT will operate. These advances together allow a wide range of new work to be done that was previously unfeasible or impossible.

4.2 Conclusions

One primary finding of this study is that results cited by Yen do not match extensive attempts to reproduce them. This is most likely due to a difference in defining the parameters of interest, especially pressure coefficient, rather than an inability to match the basic configuration of the TTWT. Although the results measured in this study are less promising than Yen's, work on aspects other than pressure coefficient measurement show that the TTWT concept is viable and promising.

The stagnation chamber can be much smaller than what is called for in the basic TTWT

configuration. A more elegant design of the interior of the chamber improves the performance of the TTWT. A smaller stagnation chamber will save on both material costs and overall size of the TTWT system.

The height-to-diameter ratio and throat hole size are not currently optimized, and changes in either of these parameters can lead to performance improvements, notwithstanding other improvements.

4.3 Recommendations

The swirl ratio is an important parameter in tornado and vortex studies. It is a measure of the ratio of tangential velocity at the edge of the vortex core to the vertical velocity through the core. The swirl ratio is a governing parameter which describes how many cells the vortex has, and what the updraft flow is like in the vortex core. Measurement of the swirl ratio and its dependence on h/D (height-to-diameter ratio of the spiral) and d_{hole}/D (ratio of throat hole diameter to spiral diameter) will be vital to finding optimal values for these ratios.

Further enhancements are possible, and vortex generators in particular should be examined. A vortex generator is an aerodynamic surface, usually a small vane, that creates a vortex. These vortex generators can be placed at various locations to inject vortex filaments into the main vortex, including on the floors and walls of the spiral chamber, as well as at the spiral chamber inlet.

More fairings for the top of the TTWT can be tested. The optimum parameters for parameters for extending the spiral chamber have not been discovered. The spiral extension can be made shorter or taller, and can follow more or less of the spiral, and can end abruptly or with a taper. More complicated fairings, like the scoop that was used initially, can be tested.

Designs to make the TTWT more omnidirectional need to be addressed. The TTWT could be installed in urban or suburban built areas which tend to channel wind in one direction, passive devices could be placed in front of the TTWT to channel the wind and increase the range of acceptable wind directions, or models with a moving tower or moveable vanes can be devised.

The stagnation chamber can be improved. Little work was done in this study to optimize its design. Many simple modifications can be made to potentially improve performance.

A better fan or extraction device should be identified to provide realistic power output. The fan used in this study was not designed to extract power from the wind. A better fan design would use both the accelerated air through the throat and the fact that the flow through the throat is already swirling to rotate a turbine.

Wind gusts and atmospheric turbulence can be modeled in wind tunnels like the AABL Wind and Gust Tunnel. Tests of the effects of these parameters on TTWT performance will demonstrate the robustness of the device and its usability in a real environment.

Parallel development of the TTWT concept with CFD should continue. Certain parameters, such as height-to-diameter ratio, are easier to change in CFD than with experimental models. This parameter, and others, can be varied to determine the dependence of TTWT performance on the parameter and thus lead to the optimal value of the parameter.

The results of this study show that the tornado-type wind turbine can be developed into a viable product for the energy market. Modern experimental techniques and facilities should be used to further refine the concept into a useable commercial product.

APPENDIX
ADDITIONAL IMPROVEMENTS TRIED

Some of the additional improvements tried that did not work are given here. Each idea is briefly described and a photo is included.

Various forms of forced inflow into the spiral chamber were attempted. The most basic form is an elbow pipe with the same diameter as the hole in the spiral chamber floor. Figure A.1 shows forced inflow that used a funnel shape to force a larger area of airflow into the pipe. A combination of forced inflow and air drawn from the stagnation chamber was tried. A Y-shaped pipe was used to allow a combination of forced air and air drawn from the stagnation chamber. Figure A.2 shows the pipe by itself. Figure A.3 shows the pipe installed in the stagnation chamber.

A small channel was installed on the wall of the chamber to direct flow at the wall up and out of the chamber. Small semi-cones were also placed at the inlet to impart spin on the incoming air. Figure A.4 shows the channel along the wall and the semi-cones at the inlet.

Semi-cones were also placed on the floor of the spiral chamber to create additional rotation at the bottom of the vortex. Figure A.5 shows these semi-cones.

Two types of floor installations were tried. One was a ramp that followed the spiral shape for one turn to start the upward flow in the vortex. Figures A.6 and A.7 show this floor installation. The other floor installation was an "inverted cone" that ran from a line around the spiral chamber to the hole in the floor, to increase the size of the spiral chamber with height. Figures A.8 and A.9 show this floor installation.

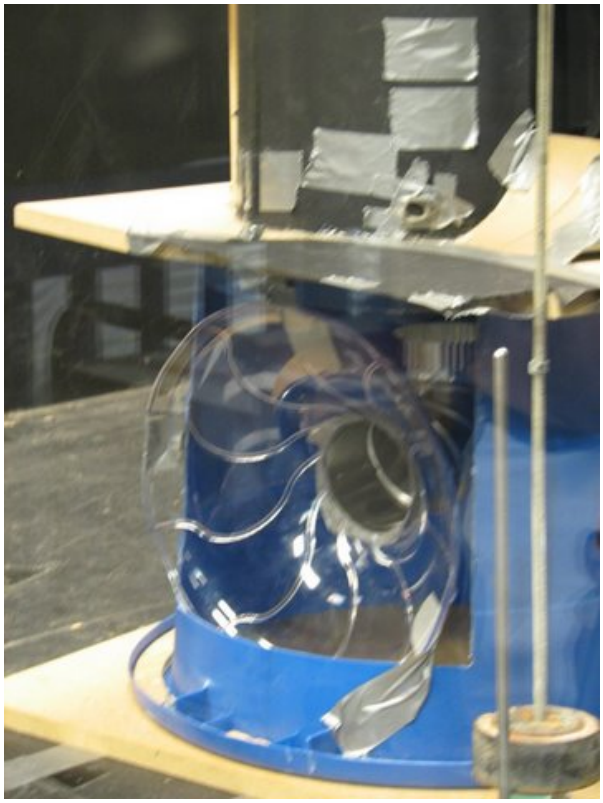

Figure A.1 Forced airflow intake to funnel a large capture area into the throat
Design modification and fabrication by J. Pierce Scarlett, photo courtesy J. Pierce Scarlett

Figure A.2 Y-shaped pipe to allow forced and drawn air through throat (inverted when installed)
Design modification and fabrication by J. Pierce Scarlett, photo courtesy J. Pierce Scarlett

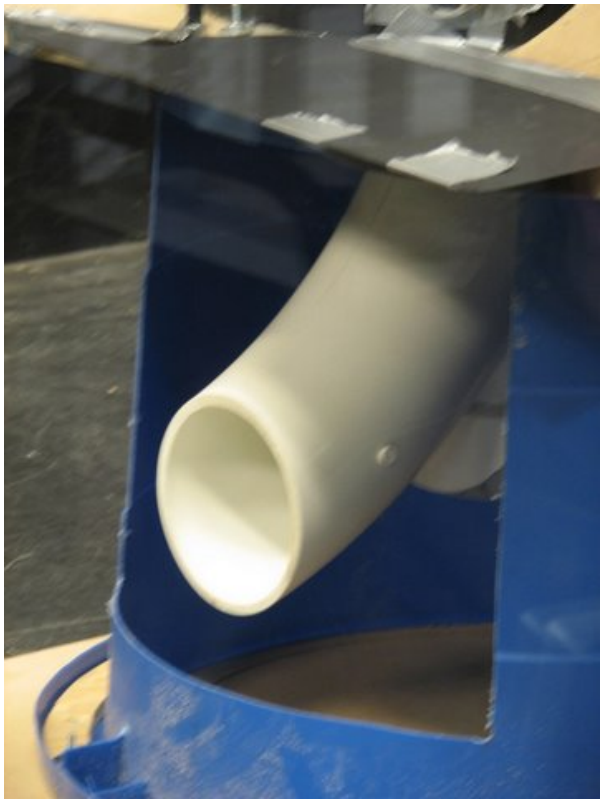

Figure A.3 Y-shaped pipe for forced and drawn air shown installed in stagnation chamber
Design modification and fabrication by J. Pierce Scarlett, photo courtesy J. Pierce Scarlett

Figure A.4 Channel along spiral wall and semi-cones at spiral inlet
Design modification and fabrication by J. Pierce Scarlett, photo courtesy J. Pierce Scarlett

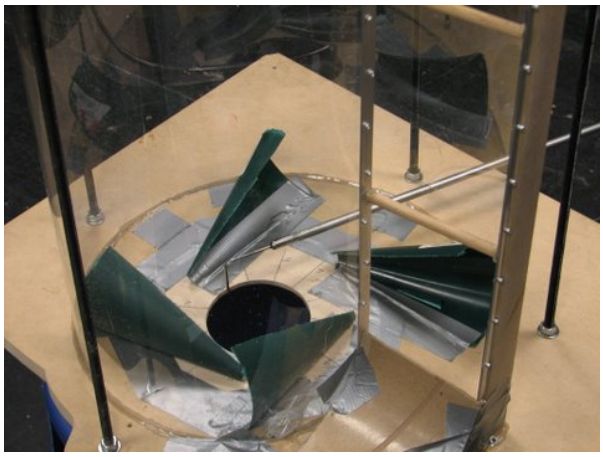

Figure A.5 Semi-cones on spiral chamber floor
Design modification and fabrication by J. Pierce Scarlett, photo courtesy J. Pierce Scarlett

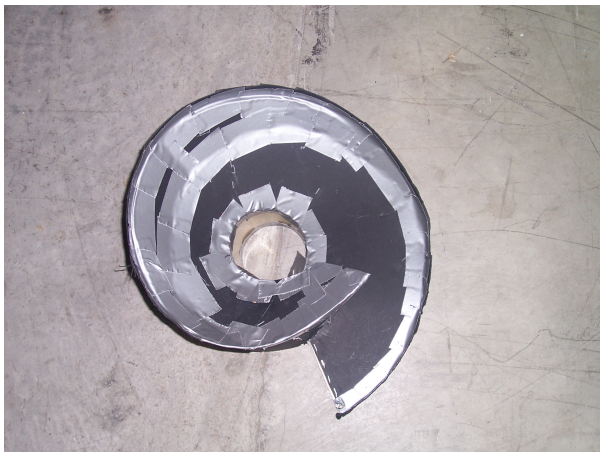

Figure A.6 Top view of ramp installation for spiral chamber floor
Design modification and fabrication by J. Pierce Scarlett, photo courtesy J. Pierce Scarlett

Figure A.7 Side view of ramp installation for spiral chamber floor
Design modification and fabrication by J. Pierce Scarlett, photo courtesy J. Pierce Scarlett

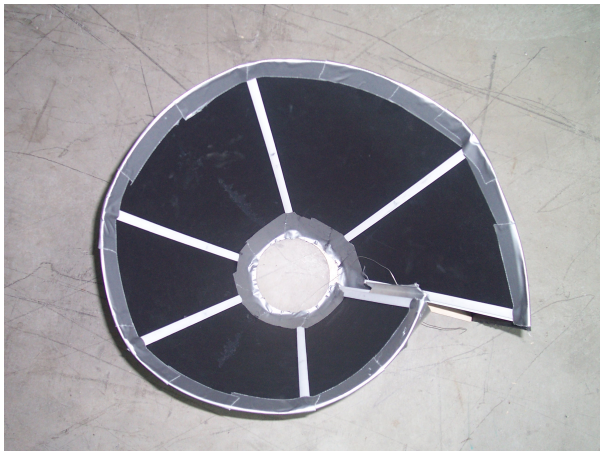

Figure A.8 Top view of inverted cone installation for spiral chamber floor Design modification and fabrication by J. Pierce Scarlett, photo courtesy J. Pierce Scarlett

Figure A.9 Side view of inverted cone installation for spiral chamber floor Design modification and fabrication by J. Pierce Scarlett, photo courtesy J. Pierce Scarlett

BIBLIOGRAPHY

[1] United States Department of Energy, office of Energy Efficiency and Renewable Energy (2008). Annual Report on U.S. Wind Power Installation, Cost, and Performance Trends:2007. Retrieved June 4, 2009 from http://www1.eere.energy.gov/windandhydro/pdfs/43025.pdf

[2] United States Department of Energy, office of Energy Efficiency and Renewable Energy (2008). 20% Wind Energy by 2030. Retrieved June 4, 2009, from http://www.20percentwind.org/20percent_wind_energy_report_revOct08.pdf

[3] National Renewable Energy Laboratory (2009). Small Wind Turbine Independent Testing. Retrieved June 8, 2009 from http://www.nrel.gov/wind/smallwind/independent_testing.html

[4] American Wind Energy Association (2008). In the Public Interest: How and Why to Permit for Small Wind Systems. Retrieved June 8, 2009 from http://www.awea.org/smallwind/pdf/InThePublicInterest.pdf

[5] American Wind Energy Association (2009). Small Wind Turbine Equipment Providers. Retrieved June 8, 2009 from http://www.awea.org/smallwind/smsyslst.html

[6] Minachi, A. (1987). Improvement of a tornado-type wind turbine in a real environment. M.S. thesis, Iowa State University, Ames, Iowa

[7] Yen, J. T. (1975). "Tornado-type Wind Energy System." Proc. 10th Inter Society Energy Conversion Engineering Conf., 987-994

[8] Yen, J. T. (1982). Investigations of the Tornago Wind Energy System Grumman Aerospace Corporation Memorandum, No. RM-643, Bethpage, New York

[9] Rangwalla, A. A. (1982). Performance and flow analysis of vortex wind power turbines. M.S. thesis, Iowa State University, Ames, Iowa

[10] Ide, H. (1982). Effect of radial inflow on vortex intensification and its application to wind vortex generators. Ph.D. thesis, Iowa State University, Ames, Iowa

[11] Mohammad, A. (2008). Numerical simulation of three dimensional vortex-dominated flows. M.S. thesis, Iowa State University, Ames, Iowa

[12] Yen, J. T. (1979). Tornado-Type Wind Energy System. Technical Status Report for the period of 27 September 1976 to 28 February 1978. Grumman Aerospace Corporation, Bethpage, New York

[13] Lugt, H. (1983). Vortex flow in nature and technology. New York: John Wiley and Sons.

[14] Tesfamariam, H. (1977). The theoretical analysis of a general vortex flow near a solid surface normal to the axis of the vortex. Iowa State University Engineering Research Institute Report, No. 77413, project No. 1123

[15] Southwest Windpower (2002). AirX Owner's Manual. Retrieved June 20, 2009 from http://www.allsmallwindturbines.com/files/airx.pdf